01 Jan 2007

Neural Network Controller Development and Implementation for Spark Ignition Engines with High EGR Levels

Jonathan B. Vance

Atmika Singh

Brian C. Kaul

Jagannathan Sarangapani
Missouri University of Science and Technology, sarangap@mst.edu

et. al. For a complete list of authors, see https://scholarsmine.mst.edu/ele_comeng_facwork/1763

Recommended Citation

J. B. Vance et al., "Neural Network Controller Development and Implementation for Spark Ignition Engines with High EGR Levels," *IEEE Transactions on Neural Networks*, Institute of Electrical and Electronics Engineers (IEEE), Jan 2007.
The definitive version is available at https://doi.org/10.1109/TNN.2007.899199

Neural Network Controller Development and Implementation for Spark Ignition Engines With High EGR Levels

Jonathan Blake Vance, *Member, IEEE*, Atmika Singh, Brian C. Kaul, Sarangapani Jagannathan, *Senior Member, IEEE*, and James A. (Jim) Drallmeier

***Abstract*—Past research has shown substantial reductions in the oxides of nitrogen (NO_x) concentrations by using 10%–25% exhaust gas recirculation (EGR) in spark ignition (SI) engines (see Dudek and Sain, 1989). However, under high EGR levels, the engine exhibits strong cyclic dispersion in heat release which may lead to instability and unsatisfactory performance preventing commercial engines to operate with high EGR levels. A neural network (NN)-based output feedback controller is developed to reduce cyclic variation in the heat release under high levels of EGR even when the engine dynamics are unknown by using fuel as the control input. A separate control loop was designed for controlling EGR levels. The stability analysis of the closed-loop system is given and the boundedness of the control input is demonstrated by relaxing separation principle, persistency of excitation condition, certainty equivalence principle, and linear in the unknown parameter assumptions. Online training is used for the adaptive NN and no offline training phase is needed. This online learning feature and model-free approach is used to demonstrate the applicability of the controller on a different engine with minimal effort. Simulation results demonstrate that the cyclic dispersion is reduced significantly using the proposed controller when implemented on an engine model that has been validated experimentally. For a single cylinder research engine fitted with a modern four-valve head (Ricardo engine), experimental results at 15% EGR indicate that cyclic dispersion was reduced 33% by the controller, an improvement of fuel efficiency by 2%, and a 90% drop in NO_x from stoichiometric operation without EGR was observed. Moreover, unburned hydrocarbons (uHC) drop by 6% due to NN control as compared to the uncontrolled scenario due to the drop in cyclic dispersion. Similar performance was observed with the controller on a different engine.**

***Index Terms*—Adaptive control, neural networks (NNs), nonlinear systems, observers, output feedback.**

NOMENCLATURE

CFR	Cooperative fuel research.
COV	Coefficient of variation.
IMEP	Mean effective pressure, Work/Disp. Volume.
NO_x	Nitrogen oxide compounds.
uHC	Unburned hydrocarbons.
$CE(k)$	Combustion efficiency.
$d_1(k)$	Unknown disturbance in air.
$d_2(k)$	Unknown disturbance in fuel.
$F(k)$	Fraction of unreacted gas and fuel remaining from previous cycle.
$r_{H_2O}(k)$	Mass of water.
$r_{O_2}(k)$	Mass of oxygen.
$r_{N_2}(k)$	Mass of nitrogen.
$r_{CO_2}(k)$	Mass of carbon dioxide.
R	Stoichiometric air–fuel mass ratio.
$u(k)$	Mass change fuel input.
$x_1(k)$	Mass of air.
$x_2(k)$	Mass of fuel.
$x_3(k)$	Mass of EGR
$\varphi(k)$	Equivalence ratio.
φ_l,φ_u	Lower 10% and upper 90% locations of the combustion efficiency function.
φ_m	Midpoint between φ_l and φ_u.

Manuscript received December 1, 2005; revised August 29, 2006; accepted February 5, 2007. This work was supported in part by the National Science Foundation under Grants ECCS#0327877 and ECCS#0621924, by the National Science Foundation I/UCRC grant on Intelligent Maintenance Systems, and by the Department of Education through GAANN program.

J. B. Vance, A. Singh, and S. Jagannathan are with the Department of Electrical and Computer Engineering, University of Missouri Rolla, Rolla, MO 65409 USA (e-mail: sarangap@umr.edu).

B. C. Kaul and J. A. Drallmeier are with the Department of Mechanical and Aerospace Engineering, University of Missouri Rolla, Rolla, MO 65409 USA.

Color versions of one or more of the figures in this paper are available online at http://ieeexplore.ieee.org.

Digital Object Identifier 10.1109/TNN.2007.899199

I. INTRODUCTION

ONE of the most interesting challenges facing the automotive industry today is the development of energy generation techniques that have a low impact on the environment. Today's automobiles utilize sophisticated microprocessor-based engine control systems to meet stringent federal regulations governing fuel economy and the emission of carbon monoxide (CO), oxides of nitrogen (NO_x) and hydrocarbons (HC). Global warming and its impact on the environment have shifted the focus of the automotive industry. Current efforts are directed at reducing the total amount of emissions and fuel consumption. The engine control system can be classified into three categories [1]: the spark advance (SA) control, the air–fuel ratio (A/F) control, and the exhaust gas recirculation (EGR) control. Partial recirculation of exhaust gases, a technique introduced in the early 1970s, has continued to receive attention [2].

Operating a spark ignition engine with EGR can reduce the NO_X as well as improve the fuel efficiency. For example, if an engine can tolerate 20%–25% EGR, reduction in engine-out NO_X on the order of 90%–95% can be realized. Additionally, improved brake specific fuel consumption with EGR dilution is a result of reduced pumping work, reduced heat transfer to the walls due to decreased burned gas temperature, and to a lesser extent, a reduction in dissociation at high temperatures in the

burned gases. EGR dilution has the advantage over lean combustion of maintaining stoichiometric operation so that current three-way catalyst technology can be used. These advantages which come with dilute engine operation are the primary motivation of this paper.

However, increased dilution of the intake charge through EGR also reduces the combustion rate, which makes stable combustion [2], [4]–[6] more difficult to achieve. High levels of EGR present in a spark ignition (SI) engine lead to cyclic dispersion in the heat release map of the SI engine. Under such conditions, a large number of misfires develop causing problems in drivability due to cycle-to-cycle variations in output as well as large increases in uHC. Therefore, commercial engines do not operate with high levels of EGR due to cyclic dispersion.

Several researchers [3], [7]–[9] have studied lean combustion engine control technology but few results have been reported for the EGR case. Investigation of the onset of complex dynamic behavior in an SI engine with high levels of simulated EGR (added nitrogen) as compared to the lean equivalence ratio case has demonstrated a bifurcation phenomenon similar to when the engine was operating under lean conditions [2]. Therefore, it is envisioned that by applying neural network (NN) controller similar to that of lean operation, the cyclic dispersion resulting from high levels of EGR dilution can be minimized, increasing the engine's EGR tolerance, potentially further reducing engine-out NO_X and unburned HC while improving fuel efficiency.

Conventional control schemes [3] have been found incapable of reducing the cyclic dispersion to the levels needed to implement these concepts. Moreover, the total amount of fuel and air in a given cylinder is normally not measurable on a per-cycle basis which necessitates the development of output feedback control schemes.

Several feedback controller designs in discrete time are proposed for the signal-input–single-out (SISO) nonlinear systems [10]–[12]. However, no output feedback control scheme currently exists for the proposed class of nonstrict feedback nonlinear discrete-time systems. No controller design is available for nonstrict feedback nonlinear systems even with state feedback. To overcome the need for complex engine dynamics and to make the controller practical, a heat release NN-based output feedback controller is proposed by using the NN universal approximation property [13].

In this paper, a direct adaptive NN controller is proposed for stable operation of the SI engine under high levels of EGR. The SI engine dynamics are modeled as a nonlinear discrete-time system in *nonstrict feedback form* [16]. The NNs are employed to learn the unknown nonlinear dynamics since the residual gas and combustion efficiency are unknown. A backstepping approach [14], [15] in discrete time is used to design the control input (injected fuel) to the total fuel system. The total fuel is then treated as the virtual control signal to the air system so that both the air and fuel states are bounded tightly to their respective targets. A separate control loop is designed for maintaining EGR levels. Consequently, the cyclic dispersion is reduced and the engine is stable even when an exact knowledge of engine dynamics is not known to the controller making the NN controller model-free.

This stability permits higher levels of diluents to be considered for a specific engine, further enhancing NO_X reduction and fuel efficiency than would be realized on an uncontrolled engine. The stability analysis of the closed-loop control system is given and the boundedness of the closed-loop signals is shown since a stable open-loop system can still become unstable with a controller. The NN weights are tuned online, with no offline learning phase required. Moreover, separation principle, persistency of excitation condition, certainty equivalence, and linear in the unknown parameters assumptions are relaxed. Performance of the NN controller is evaluated on different engines and results show satisfactory performance of the controller.

II. Engine as a Nonlinear Discrete-Time System

A. Nonstrict Nonlinear System Description

Consider the following nonstrict feedback nonlinear system described by the following:

$$x_1(k+1) = f_1(x_1(k), x_2(k)) + g_1(x_1(k), x_2(k))\, x_2(k) + d_1(k) \tag{1}$$

$$x_2(k+1) = f_2(x_1(k), x_2(k)) + g_2(x_1(k), x_2(k))\, u(k) + d_2(k) \tag{2}$$

where $x_i(k) \in \Re$, $i = 1, 2$, are states, $u(k) \in \Re$ is the system input, and $d_1(k) \in \Re$ and $d_2(k) \in \Re$ are unknown but bounded disturbances. Bounds on these disturbances are given by $|d_1(k)| < d_{1m}$ and $|d_2(k)| < d_{2m}$ where d_{1m} and d_{2m} are unknown positive scalars.

Equations (1) and (2) represent a discrete-time nonlinear system in nonstrict feedback form [16], since $f_1(\cdot)$ and $g_1(\cdot)$ are functions of both $x_1(k)$ and $x_2(k)$, unlike in the case of strict feedback nonlinear system, where $f_1(\cdot)$ and $g_1(\cdot)$ are a function of $x_1(k)$ only [10]–[12]. Control of nonstrict feedback nonlinear systems is introduced in [16] since no known results are available in the literature. Controller results from strict feedback nonlinear systems cannot be directly extended to nonstrict feedback nonlinear systems due to noncausal controller design issues. Next, the engine dynamics are presented in the nonstrict feedback form and, subsequently, the NN controller development is introduced. The dynamic NN architecture acts as a one-step predictor overcoming the noncausal design. The SI engine dynamic model is discussed next.

B. Engine Dynamics

Daw *et al.* [4] and Daw *et al.* [5] developed a mathematical representation of the SI engine to investigate nonlinear cycle dynamics under lean conditions and high EGR levels [2]. The residual air and fuel passed from one cycle to the next make the model deterministic. Actual variations in parameters due to complex processes such as temperature and pressure effects, turbulence, fuel vaporization, etc., are not directly calculated, but modeled as stochastic effects through random noise on parameters such as injected A/F ratio and residual fraction. The model

for the EGR case is shown as follows:

$$x_1(k+1)=F(k)\,[x_1(k)-R.\mathrm{CE}(k)x_2(k)+r_{\mathrm{O}_2}(k)+r_{\mathrm{N}_2}(k)]+x_{1\mathrm{new}}(k)+d_1(k) \quad (3)$$

$$x_2(k+1)=F(k)\,(1-\mathrm{CE}(k))\,x_2(k)+x_{2\mathrm{new}}(k)+u(k)+d_2'(k) \quad (4)$$

$$x_3(k+1)=F(k)\,(r_{\mathrm{CO}_2}(k)+r_{\mathrm{H}_2\mathrm{O}}(k)+r_{\mathrm{N}_2}(k)+x_3(k)+\mathrm{EGR}(k)) \quad (5)$$

$$y(k)=x_2(k)\mathrm{CE}(k) \quad (6)$$

$$\varphi(k)=R\frac{x_2(k)}{x_1(k)}\cdot\left[1-\gamma\frac{x_3(k)+\mathrm{EGR}(k)}{(x_2(k)+x_1(k)+x_3(k)+\mathrm{EGR}(k))}\right] \quad (7)$$

$$\mathrm{CE}(k)=\frac{\mathrm{CE}_{\max}}{1+100^{-(\varphi(k)-\varphi_m)/(\varphi_u-\varphi_l)}}\qquad \varphi_m=\frac{\varphi_u+\varphi_l}{2} \quad (8)$$

$$r_{\mathrm{H}_2\mathrm{O}}(k)=\gamma_{\mathrm{H}_2\mathrm{O}}x_2(k)\mathrm{CE}(k) \quad (9)$$

$$r_{\mathrm{O}_2}(k)=\gamma_{\mathrm{O}_2}x_2(k)\mathrm{CE}(k) \quad (10)$$

$$r_{\mathrm{N}_2}(k)=\gamma_{\mathrm{N}_2}R.x_2(k)\mathrm{CE}(k) \quad (11)$$

$$r_{\mathrm{CO}_2}(k)=\gamma_{\mathrm{CO}_2}x_2(k)\mathrm{CE}(k). \quad (12)$$

Equations for $x_1(k)$, $x_2(k)$, and $x_3(k)$ are the total mass of air, fuel, and inert gases, respectively. The heat release at the kth time instant is assumed to be proportional to the mass of fuel burned, which is given by $y(k)$. The term $\mathrm{CE}(k)$ is defined as the combustion efficiency, which is bounded above as $0 < \mathrm{CE}_{\min} < \mathrm{CE}(k) < \mathrm{CE}_{\max}$ where $\mathrm{CE}_{\max}$ is the maximum combustion efficiency denoted here as a constant. The term $F(k)$ is the residual gas fraction, which is bounded as $0 < F_{\min} < F(k) < F_{\max}$ whereas R is the stoichiometric A/F ratio, which is given by $\approx$15.13 for iso-octane. The term $u(k)$ is the small change in fuel per cycle and $\varphi(k)$ is the equivalence ratio. Additionally, φ_l, φ_u, and φ_m are equivalence ratio system parameters for the lower 10%, upper 90%, and midpoint locations of the combustion efficiency function. The terms $r_{\mathrm{H}_2\mathrm{O}}(k)$, $r_{\mathrm{O}_2}(k)$, $r_{\mathrm{N}_2}(k)$, and $r_{\mathrm{CO}_2}(k)$ are the mass of water, oxygen, nitrogen, and carbon dioxide, respectively.

It should be noted that the residual oxygen combines proportionally with the residual nitrogen to form residual air. The fraction of total nitrogen left over after this is the residual inert nitrogen. The terms γ, $\gamma_{\mathrm{H}_2\mathrm{O}}$, γ_{O_2}, γ_{N_2}, and γ_{CO_2} are constant parameters which are determined from stoichiometry and fuel properties such as the hydrogen/carbon ratio and the molecular weight. The terms $d_1'(k)$ and $d_2'(k)$ are unknown, bounded disturbances. It can be seen that the SI engine with EGR levels has highly nonlinear dynamics with $\mathrm{CE}(k)$ and $F(k)$ being unknown and not measurable.

Remark 1: In (3)–(6), states $x_1(k)$ and $x_2(k)$ are not available for feedback control since they are not measured whereas the output $y(k)$ is available for measurement. Then, the control objective is to operate the engine with high EGR levels with $y(k)$ as the feedback parameter and without knowing precisely the engine dynamics. It is important to note that the output is a nonlinear function of the states unlike in many papers [10], [11] where the output is considered as a linear function of system states.

Remark 2: For lean engine operation, the inert gas (5) is not required and, therefore, fewer parameters are in (3) and (4).

C. Engine Dynamics Using Nominal Values

Substituting (4) into both (3) and (4), we get

$$x_1(k+1)=F(k)\,[x_1(k)-R.y(k)+r_{\mathrm{O}_2}(k)+r_{\mathrm{N}_2}(k)]+x_{1\mathrm{new}}(k)+d_1(k) \quad (13)$$

$$x_2(k+1)=F(k)\,(x_2(k)-y(k))+x_{2\mathrm{new}}(k)+u(k)+d_2'(k). \quad (14)$$

In real engine operation, the fresh air $x_{1\mathrm{new}}$, fresh fuel, $x_{2\mathrm{new}}$, and residual gas fraction $F(k)$ can all be viewed as nominal values plus some small and bounded disturbances. The inert gases include the residual exhaust gases in the cylinder and the EGR fraction. Equation (5) will not be considered for controller development as a separate control loop from the literature designed to control EGR levels makes the inert gases evolve into a stable value. One can observe that (5) is a stable system and standard control results [17] can be applied. Therefore, it is sufficient to use (3) and (4) in order to minimize cyclic dispersion and (5) is not included in the proposed controller design.

Consider

$$x_{1\mathrm{new}}(k)=x_{1\mathrm{new}0}+\Delta x_{1\mathrm{new}}(k) \quad (15)$$

$$x_{2\mathrm{new}}(k)=x_{2\mathrm{new}0}+\Delta x_{2\mathrm{new}}(k) \quad (16)$$

$$F(k)=F_0(k)+\Delta F(k) \quad (17)$$

where $x_{1\mathrm{new}0}$, $x_{2\mathrm{new}0}$, and F_0 are the known nominal fresh air, fuel, and residual gas fraction values. $\Delta x_{1\mathrm{new}0}$, $\Delta x_{2\mathrm{new}0}$, and ΔF_0 are unknown yet bounded disturbances on those values whose bounds are given by

$$0 \le |\Delta x_{1\mathrm{new}}(k)| \le \Delta x_{1\mathrm{new}M} \quad (18)$$

$$0 \le |\Delta x_{2\mathrm{new}}(k)| \le \Delta x_{2\mathrm{new}M} \quad (19)$$

$$0 \le |\Delta F(k)| \le \Delta F_M. \quad (20)$$

Substituting these values into the system model, we can get the state equations in the following form:

$$x_1(k+1)=(F_0(k)+\Delta F(k))\,[x_1(k)-R.\mathrm{CE}(k)x_2(k)+r_{\mathrm{O}_2}(k)+r_{\mathrm{N}_2}(k)]+x_{1\mathrm{new}0}+\Delta x_{1\mathrm{new}}(k)+d_1(k) \quad (21)$$

$$x_2(k+1)=(F_0(k)+\Delta F(k))\,(1-\mathrm{CE}(k))\,x_2(k)+x_{2\mathrm{new}0}+\Delta x_{2\mathrm{new}}(k)+u(k)+d_2'(k). \quad (22)$$

It is important to note that the closed-loop stability analysis has to be performed with the proposed NN controller even though many of the engine terms are considered bounded above since a stable open-loop system can still become unstable with a controller unless the NN weight update laws are properly selected. Moreover, a Lyapunov-based stability analysis is needed in order to show the relaxation of the separation principle for the observer and certainty equivalence principle for the controller. Next, the NN observer design is introduced.

III. NN-Based Observer Design

First, a semirecurrent NN is used to predict the value of the heat release for the next burn cycle, which will be used subsequently by the observer to predict the states of the system. The inert gases can be calculated directly if the air and fuel values are known, so they are not estimated. The heat release for the next burn cycle is given by

$$y(k+1) = x_2(k+1)\mathrm{CE}(k+1). \tag{23}$$

A. Observer Structure

From (23), the heat release for the next cycle $y(k+1)$ can be approximated by using a one layer neural network as

$$y(k+1) = w_1^T \phi_1\left(v_1^T z_1(k)\right) + \varepsilon_1\left(z_1(k)\right) \tag{24}$$

where the input to the NN is taken as $z_1(k) = [x_1(k), x_2(k), y(k), u(k)]^T \in R^4$, the matrix $w_1 \in R^{4\times n_1}$ and $v_1 \in R^{4\times n_1}$ represent the output and hidden layer weights, $\phi_1(.)$ represents the hidden layer activation function, n_1 denotes the number of the nodes in the hidden layer, and $\varepsilon_1(z_1(k)) \in R$ is the functional approximation error. It has been demonstrated that if the hidden layer weight v_1 is chosen initially at random and held constant, and the number of hidden layer nodes is sufficiently large, then the approximation error $\varepsilon_1(z_1(k))$ can be made arbitrarily small over the compact set since the activation functions form a basis according to [13].

For simplicity, we define

$$\phi_1\left(z_1(k)\right) = \phi_1\left(v_1^T z_1(k)\right) \tag{25}$$

$$\varepsilon_1(k) = \varepsilon_1\left(z_1(k)\right). \tag{26}$$

Given (24)–(26) is rewritten as

$$y(k+1) = w_1^T \phi_1\left(z_1(k)\right) + \varepsilon_1(k). \tag{27}$$

Since states $x_1(k)$ and $x_2(k)$ are not measurable, $z_1(k)$ is not available either. Using the estimated values $\hat{x}_1(k)$, $\hat{x}_2(k)$, and $\hat{y}(k)$ instead of $x_1(k)$, $x_2(k)$, and $y(k)$, the proposed heat release observer can be given as

$$\begin{aligned}\hat{y}(k+1) &= \hat{w}_1^T \phi_1\left(v_1^T \hat{z}_1(k)\right) + l_1 \tilde{y}(k) \\ &= \tilde{w}_1^T(k)\phi_1\left(\hat{z}_1(k)\right) + l_1\tilde{y}(k)\end{aligned} \tag{28}$$

where $\hat{y}(k+1)$ is the predicted heat release, $\hat{w}_1(k) \in R^{n_i}$ is the actual output layer weights, the input to the NN is taken as $\hat{z}_1(k) = [\hat{x}_1(k), \hat{x}_2(k), \hat{y}(k), u(k)]^T \in R^4, l \in R$ is the observer gain, $\tilde{y}(k)$ is the heat release estimation error, which is defined as

$$\tilde{y}(k) = \hat{y}(k) - y(k) \tag{29}$$

and $\phi_1(\hat{z}_1(k))$ represents $\phi_1(v_1^T \hat{z}_1(k))$ for the purpose of simplicity.

Using the heat release estimation error, the proposed observer is given in the following form:

$$\hat{x}_1(k+1) = x_{1\mathrm{new}0}(k) + F_o \hat{x}_1(k) - R \cdot F_o \cdot \hat{y}(k) + l_2 \tilde{y}(k) \tag{30}$$

$$\hat{x}_2(k+1) = F_o\left(\hat{x}_2(k) - \hat{y}(k)\right) + \left(x_{2\mathrm{new}0}(k) + u(k)\right) + l_3\tilde{y}(k) \tag{31}$$

where $l_2 \in R$ and $l_3 \in R$ are observer gains. The term $F_o(r_{\mathrm{O}_2} + r_{\mathrm{N}_2})$ has been pulled out from (30) as there are no nominal values available for the inert gases. The error introduced by this will be taken up as part of the air estimation error. Equations (26), (28), and (29) represent the dynamics of the observer to estimate the states of $x_1(k)$ and $x_2(k)$.

B. Observer Error Dynamics

Define the state estimation errors as

$$\tilde{x}_i(k) = \hat{x}_i(k) - x_i(k), \qquad i = 1, 2. \tag{32}$$

Combining (21)–(26), we obtain the estimation error dynamics as

$$\begin{aligned}\tilde{x}_1(k+1) = {} & F_o\tilde{x}_1(k) + (l_2 - R \cdot F_o)\tilde{y}(k) - \Delta x_{1\mathrm{new}}(k) \\ & - \Delta F(k)x_1(k) + R\Delta F(k)y(k) \\ & - F_o\left(r_{\mathrm{O}_2} + r_{\mathrm{N}_2}\right) - \Delta F\left(r_{\mathrm{O}_2} + r_{\mathrm{N}_2}\right) \\ & - d_1(k)\end{aligned} \tag{33}$$

$$\begin{aligned}\tilde{x}_2(k+1) = {} & F_o\tilde{x}_2(k) + (l_3 - F_o)\tilde{y}(k) \\ & - \Delta F(k)\left(x_2(k) - y(k)\right) - \Delta x_{2\mathrm{new}}(k) \\ & - d_2(k)\end{aligned} \tag{34}$$

$$\begin{aligned}\tilde{y}(k+1) = {} & \hat{w}_1^T(k)\phi_1\left(\hat{z}_1(k)\right) + l_1\tilde{y}(k) \\ & - w_1^T\phi_1\left(z_1(k)\right) - \varepsilon_1(k) \\ = {} & \left(\hat{w}_1(k) - w_1\right)^T \phi_1\left(\hat{z}_1(k)\right) \\ & + w_1^T\left(\phi_1\left(\hat{z}_1(k)\right) - \phi_1\left(z_1(k)\right)\right) - \varepsilon_1(k) \\ = {} & \tilde{w}_1^T(k)\phi_1\left(\hat{z}_1(k)\right) + \tilde{w}_1^T(k)\phi_1\left(\tilde{z}_1(k)\right) - \varepsilon_1(k) \\ = {} & \zeta_1(k) + w_1^T\phi_1\left(\tilde{z}_1(k)\right) - \varepsilon_1(k)\end{aligned} \tag{35}$$

where

$$\tilde{w}_1(k) = \hat{w}_1(k) - w_1 \tag{36}$$

and

$$\zeta_1(k) = \tilde{w}_1^T(k)\phi_1\left(\hat{z}_1(k)\right) \tag{37}$$

and for the purpose of simplicity, $(\phi_1(\hat{z}_1(k)) - \phi_1(z_1(k)))$ is written as $(\phi_1(\tilde{z}_1(k))$. Next, the NN controller design is presented and the NN weight updates for both NN observer and controller are discussed.

IV. Adaptive NN Output Feedback Controller Design

The control objective of maintaining the heat release constant is achieved by holding the fuel and combustion efficiency within a close bound, i.e., the heat release is driven to a target heat release y_d. Given y_d and the engine dynamics (3)–(5), we could obtain the nominal values for the total mass of air and fuel in the cylinder x_{1d} and x_{2d}, respectively. By driving the states $x_1(k)$ and $x_2(k)$ to approach their respective nominal values x_{1d} and x_{2d}, $y(k)$ will approach y_d. By developing a controller to maintain the EGR at a constant level separately, we can see that the inert gases evolve into a stable value since (5) can be viewed as a feedback linearizable nonlinear discrete-time system with $F(k)$

being less than one and the weights of the gases kept constant with minor variations. The controller for the EGR system (5) is developed separately and not presented here. With the estimated states $\hat{x}_1(k)$ and $\hat{x}_2(k)$, the controller design follows the backstepping technique [14], [15]. The details are given in the following sections.

A. Adaptive NN Output Feedback Controller Design

The controller design is now given.

Step 1) Virtual controller design.

Define the error between actual and desired air as

$$e_1(k) = x_1(k) - x_{1d} \tag{38}$$

which can be rewritten as

$$\begin{aligned} e_1(k+1) =& x_1(k+1) - x_{1d} \\ =& F(k)\left[x_1(k) - R.\mathrm{CE}(k)x_2(k)\right. \\ &\left. + r_{\mathrm{O}_2}(k) + r_{\mathrm{N}_2}(k)\right] - x_{1d} + x_{1\mathrm{new}}(k) \\ &+ d_1(k). \end{aligned} \tag{39}$$

For simplicity, let us denote

$$\begin{aligned} f_1(k) =& F(k)\left[x_1(k) + r_{\mathrm{O}_2}(k) + r_{\mathrm{N}_2}(k)\right] \\ &+ x_{1\mathrm{new}}(k) - x_{1d} \end{aligned} \tag{40}$$

$$g_1(k) = R \cdot F(k)\mathrm{CE}(k). \tag{41}$$

Then, the system error equation can be expressed as

$$e_1(k+1) = f_1(k) - g_1(k)x_2(k) + d_1(k). \tag{42}$$

By viewing $x_2(k)$ as a virtual control input, a desired feedback control signal can be designed as

$$x_{2d}(k) = \frac{f_1(k)}{g_1(k)}. \tag{43}$$

The term x_{2d} can be approximated by the first action NN as

$$\begin{aligned} x_{2d}(k) =& w_2^T \phi_2\left(v_2^T x(k)\right) + \varepsilon_2\left(x(k)\right) \\ =& w_2^T \phi_2\left(x(k)\right) + \varepsilon_2\left(x(k)\right) \end{aligned} \tag{44}$$

where the inputs in the state $x(k) = [x_1(k), x_2(k)]^T$, $w_2 \in R^{n_2}$, and $v_2 \in R^{2\times n_1}$ denote the constant ideal output and hidden layer weights, n_2 is the number of nodes in the hidden layer, the hidden layer activation function $\phi_2(v_2^T x(k))$ is simplified as $\phi_2(x(k))$, and $\varepsilon_2(x(k))$ is the approximation error. Since both $x_1(k)$ and $x_2(k)$ are unavailable, the estimated state $\hat{x}(k)$ is selected as the NN input.

Consequently, the virtual control input is taken as

$$\hat{x}_{2d}(k) = \hat{w}_2^T(k)\phi_2\left(v_2^T\hat{x}(k)\right) = \hat{w}_2^T(k)\phi_2\left(\hat{x}(k)\right) \tag{45}$$

where $\hat{w}_2(k) \in R^{n_2}$ is the actual weight matrix for the first control NN. Define the weight estimation error by

$$\tilde{w}_2(k) = \hat{w}_2(k) - w_2. \tag{46}$$

Define the error between $x_2(k)$ and $\hat{x}_{2d}(k)$ as

$$e_2(k) = x_2(k) - \hat{x}_{2d}(k). \tag{47}$$

Equation (35) can be expressed using (47) for $x_2(k)$ as

$$e_1(k+1) = f_1(k) - g_1(k)\left(e_2(k) + \hat{x}_{2d}(k)\right) + d_1(k) \tag{48}$$

or, equivalently

$$\begin{aligned} e_1(k+1) =& f_1(k) - g_1(k)\left(e_2(k) + x_{2d}(k) - x_{2d}(k) + x_{2d}(k)\right) \\ &+ d_1(k) \\ =& f_1(k) - g_1(k)\left(e_2(k) + x_{2d}(k) - x_{2d}(k) + \hat{x}_{2d}(k)\right) \\ &+ d_1(k) \\ =& -g_1(k)\left(e_2(k) - x_{2d}(k) + \hat{x}_{2d}(k)\right) + d_1(k) \\ =& -g_1(k)\left(e_2(k) + \hat{w}_2^T(k)\phi_2\left(\hat{x}(k)\right)\right. \\ &\left. - w_2^T\phi_2\left(x(k)\right) - \varepsilon_2\left(x(k)\right)\right) \\ &+ d_1(k). \end{aligned} \tag{49}$$

Similar to (35), (49) can be further expressed as

$$\begin{aligned} e_1(k+1) = -g_1(k)\left(e_2(k) - \zeta_2(k) + w_2^T\phi_2\left(\tilde{x}(k)\right)\right. \\ \left. - \varepsilon_2\left(x(k)\right)\right) + d_1(k) \end{aligned} \tag{50}$$

where

$$\zeta_2(k) = \tilde{w}_2^T(k)\phi_2\left(\hat{x}(k)\right) \tag{51}$$

$$w_2^T\phi_2\left(\tilde{x}(k)\right) = w_2^T\left(\phi_2\left(\hat{x}(k)\right) - \phi_2\left(x(k)\right)\right). \tag{52}$$

Step 2) Design of the control input $u(k)$.

We rewrite the error $e_2(k)$ from (47) as

$$\begin{aligned} e_2(k+1) =& x_2(k+1) - \tilde{x}_{2d}(k+1) \\ =& \left(1 - \mathrm{CE}(k)\right)F(k)x_2(k) + \left(MF(k) + u(k)\right) \\ &- \hat{x}_{2d}(k+1) + d_2(k). \end{aligned} \tag{53}$$

For simplicity, let us denote

$$x_2(k+1) = F(k)\left(1 - \mathrm{CE}(k)\right)x_2(k) + x_{2\mathrm{new}}(k). \tag{54}$$

Equation (53) can be written as

$$e_2(k+1) = f_2(k) + u(k) - \hat{x}_{2d}(k+1) + d_2(k) \tag{55}$$

where $\hat{x}_{2d}(k+1)$ is the future value of $\hat{x}_{2d}(k)$. Here, $\hat{x}_{2d}(k+1)$ is not available in the current time step. However, from (43) and (45), it can be clear that $\hat{x}_{2d}(k+1)$ is a smooth nonlinear function of the state $x(k)$ and virtual control input $\hat{x}_{2d}(k)$. Another NN can be used to approximate the value of $\hat{x}_{2d}(k+1)$ and to generate a suitable control input by using this

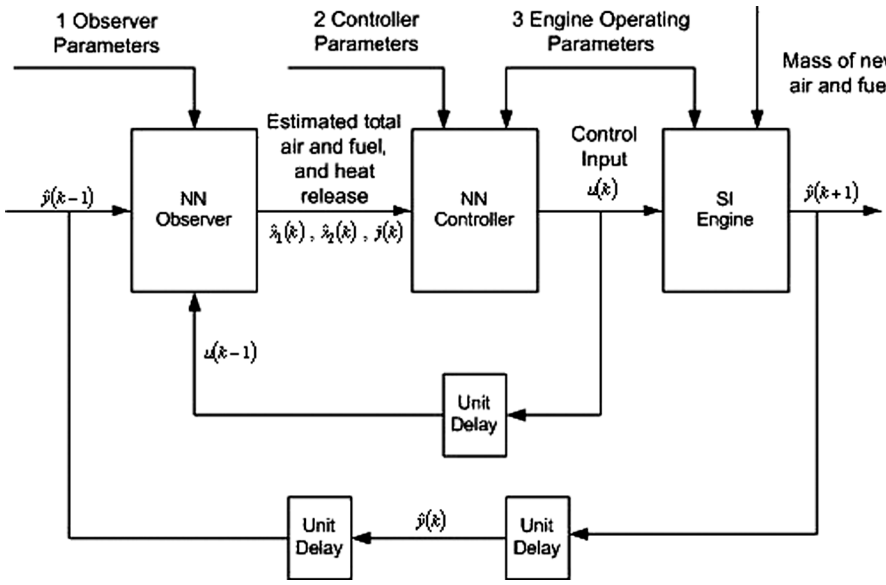

Fig. 1. Neurocontroller structure.

value since a second control NN with semirecurrent architecture can be viewed as a first-order predictor. Other methods via filtering approach [18] do exist in the literature in order to obtain this future value which can subsequently be used by a second control NN.

Select the desired control input by using the second NN in the controller design as

$$\begin{aligned} u_d(k) &= (-f_2(k) + \hat{x}_{2d}(k+1)) \\ &= w_3^T \phi_3\left(v_3^T z_3(k)\right) + \varepsilon_3\left(z_3(k)\right) \\ &= w_3^T \phi_3\left(z_3(k)\right) + \varepsilon_3\left(z_3(k)\right) \end{aligned} \tag{56}$$

where $w_3 \in R^{n_3}$ and $v_3 \in R^{3\times n_3}$ denote the constant ideal output and hidden layer weights, n_3 is the hidden layer nodes number, the hidden layer activation function $\phi_3(v_3^T z_3(k))$ is simplified as $\phi_3(z_3(k))$, $\varepsilon_3(z_3(k))$ is the approximation error, and $z_3(k) \in R^3$ is the NN input, which is given by (55). Considering the fact that both $x_1(k)$ and $x_2(k)$ cannot be measured, $z_3(k)$ is substituted with $\hat{z}_3(k) \in R^3$ where

$$z_3(k) = [x(k), \hat{x}_{2d}(k)]^T \in R^3 \tag{57}$$

and

$$\hat{z}_3(k) = [\hat{x}(k), \hat{x}_{2d}(k)]^T \in R^3. \tag{58}$$

Now, define

$$\hat{e}_1(k) = \hat{x}_1(k) - x_{1d} \tag{59}$$

and

$$\hat{e}_2(k) = \hat{x}_2(k) - x_{2d}. \tag{60}$$

The actual control input is now selected as

$$\begin{aligned} u(k) &= \hat{w}_3^T(k)\phi_3\left(v_c^T \hat{z}_3(k)\right) + l_4 \hat{e}_2(k) \\ &= \hat{w}_3^T(k)\phi_3\left(\hat{z}_3(k)\right) + l_4 \hat{e}_2(k) \end{aligned} \tag{61}$$

where $\hat{w}_3^T \in R^{n_3}$ is the actual output layer weights and $l_4 \in R$ is the controller gain selected to stabilize the system. Similar to the derivation of (39), combining (55) and (56) with (61) yields

$$e_2(k+1) = l_4 \hat{e}_2(k) + \xi_3(k) + w_3^T \phi_3\left(\tilde{z}(k)\right) - \varepsilon_3\left(z_3(k)\right) + d_2(k) \tag{62}$$

where

$$\tilde{w}_3(k) = \hat{w}_3(k) - w_3 \tag{63}$$

$$\xi_3(k) = \tilde{w}_3^T(k)\phi_3\left(\hat{z}_3(k)\right) \tag{64}$$

and

$$w_3^T \phi_3\left(\tilde{z}(k)\right) = w_3^T\left(\phi_3\left(\hat{z}_3(k)\right) - \phi_3\left(z_3(k)\right)\right). \tag{65}$$

Equations (50) and (62) represent the closed-loop error dynamics. It is required to show that the estimation error (29) and (32), the system errors (50) and (62), and the NN weight matrices $\hat{w}_1(k)$, $\hat{w}_2(k)$, and $\hat{w}_3(k)$ are bounded. Fig. 1 shows the block diagram of the final structure of the designed neurocontroller.

B. Weight Updates for Guaranteed Performance

Assumption 1 (Bounded Ideal Weights): Let w_1, w_2, and w_3 be the unknown output layer target weights for the observer and two action NNs and assume that they are bounded above so that

$$\|w_1\| \le \|w_{1m}\|, \|w_2\| \le \|w_{2m}\|, \text{ and } \|w_3\| \le \|w_{3m}\| \tag{66}$$

where $w_{1m} \in R^+$, $w_{2m} \in R^+$, and $w_{3m} \in R^+$ represent the bounds on the unknown target weights when the Frobenius norm is used.

Fact 1: The activation functions are bounded above by known positive values so that

$$\|\phi_i(\cdot)\| \leq \phi_{im}, \qquad i = 1,2,3 \tag{67}$$

where ϕ_{im}, $i = 1,2,3$, are the upper bounds.

Assumption 2 (Bounded NN Approximation Error): The NN approximation errors $\varepsilon_1(z_1(k))$, $\varepsilon_2(x(k))$, and $\varepsilon_3(z_3(k))$ are bounded over the compact set by ε_{1m}, ε_{2m}, and ε_{3m}, respectively.

Theorem 1: Consider the system given in (3)–(5) and let the Assumptions 1 and 2 hold. Let the unknown disturbances be bounded by $|d_1(k)| \leq d_{1m}$ and $|d_2(k)| \leq d_{2m}$, respectively. Let the observer NN weight tuning be given by

$$\hat{w}_1(k+1) = \hat{w}_1(k) - \alpha_1 \phi_1(\hat{z}_1(k)) \left(\hat{w}_1^T(k)\phi_1(\hat{z}_1(k) + l_5\tilde{y}(k)\right) \tag{68}$$

with the virtual control NN weight tuning being provided by

$$\hat{w}_2(k+1) = \hat{w}_2(k) - \alpha_2 \phi_2(\hat{x}(k)) \left(\hat{w}_2^T(k)\phi_2(\hat{x}(k) + l_6\hat{e}_1(k)\right) \tag{69}$$

and the control NN weight tuning be provided by

$$\hat{w}_3(k+1) = \hat{w}_3(k) - \alpha_3 \phi_3(\hat{z}_3(k)) \left(\hat{w}_3^T(k)\phi_3(\hat{z}_3(k) + l_7\hat{e}_2(k)\right) \tag{70}$$

where $\alpha_1 \in R$, $\alpha_2 \in R$, and $\alpha_3 \in R$, and $l_5 \in R$, $l_6 \in R$, and $l_7 \in R$ are design parameters. Let the system observer be given by (28)–(30) and virtual and actual control inputs be defined as (45) and (61), respectively. The estimation errors (33)–(35), the tracking errors (50) and (62), and the NN weight estimates $\hat{w}_1(k)$, $\hat{w}_2(k)$, and $\hat{w}_3(k)$ are uniformly ultimately bounded (UUB) with the bounds specifically given by (A.17)–(A.20) provided the design parameters are selected as follows:

1)

$$0 < \alpha_i \|\phi_i(k)\|^2 < 1, \qquad i = 1,2,3; \tag{71}$$

2)

$$l_3^2 < 1 - \frac{(l_1 - R \cdot F_0)^2}{6R^2 \cdot \Delta F_m^2} - \frac{(l_2 - F_0)^2}{6\Delta F_m^2} - 4l_5^2; \tag{72}$$

3)

$$l_6^2 < \min\left(\frac{\left(1 - F_0^2\right)}{18R^2 \cdot \Delta F_m^2}, \frac{1}{18R^2}\right); \tag{73}$$

4)

$$l_4^2 + 6l_7^2 < \min\left(\frac{\left(1 - F_0^2\right)}{6\Delta F_m^2}, \frac{1}{3}\right). \tag{74}$$

Proof: See the Appendix.

Remark 3: For general nonlinear discrete-time systems, the design parameters can be selected using *a priori* values. Given specific values of R, F_0, and ΔF_m, the design parameters can be derived as l_i, $i = 1$ to 7. For instance, given $R = 14.6$, $F_0 = 0.14$, and $\Delta F_m = 0.02$, we can select $l_1 = 1.99$, $l_2 = 0.13$, $l_3 = 0.4$, $l_4 = 0.14$, $l_5 = 0.25$, $l_6 = 0.016$, and $l_7 = 0.1667$ to satisfy (71)–(74).

Remark 4: A well-defined controller is developed in this paper since a single NN is utilized to approximate two nonlinear functions, thereby avoiding division by zero.

Remark 5: It is important to note that in this theorem there is no persistency of excitation condition (PE) condition for the NN observer and NN controller in contrast with standard work in the discrete-time adaptive control [19] since the first difference of the Lyapunov function in the Appendix does not require the PE condition on input signals to prove the boundedness of the weights. Even though the input to the hidden-layer weight matrix is not updated and only the hidden-to-the-output-layer weight matrix alone is tuned, the NN method relaxes the linear in the unknown parameter assumption. Additionally, certainty equivalence principle is not used in the proof.

Remark 6: Generally, the separation principle used for linear systems does not hold for nonlinear systems, and hence, it is relaxed in this paper for the controller design since the Lyapunov function is a quadratic function of system errors and weight estimation errors of the observer and controller NNs.

Remark 7: It is important to notice that the NN outputs are not fed as delayed inputs to the network whereas the outputs of each layer are fed as delayed inputs to the same layer. The NN weight tuning proposed in (68)–(70) render a semirecurrent architecture due to the proposed weight tuning law even though feedforward NNs are utilized in the observer and controller. This semirecurrent NN architecture renders a dynamic NN which is capable of predicting the state one step-ahead overcoming the noncausal controller design.

V. Simulation Results

In an initial phase to test the effectiveness of the control scheme, the Daw model was used to simulate the engine dynamics under high levels of diluent. The model input parameters were calibrated by comparing return maps of heat release to return maps from the single cylinder engines discussed in Section VI. This approach, used in prior lean combustion work [9], provided a basis for choosing the nominal input mass of fuel and air as well as the residual gas fraction and stochastic variation. The controller was then applied to the simulation model to investigate the reduction in cyclic variability.

The simulation parameters selected were as follows: An equivalence ratio of one was maintained with stochastic variation of 1%, R $= 15.13$ for iso-octane, residual gas fraction F $= 0.09$, mass of nominal new air $= 0.52485$, mass of nominal new fuel $= 0.02428$, the standard deviation of mass of new fuel is 0.007, cylinder volume in moles $= 0.021$, molecular weight of fuel $= 114$, molecular weight of air $= 28.84$, $\phi_u = 0.665$, $\phi_l = 0.645$, maximum combustion efficiency $= 1$, and the gains (l_1, l_2) of backstepping controller are selected at 0.1 and placed diagonally to satisfy (72)–(74). The EGR was assumed to be an inert mixture with a molecular weight of 30.4. The residuals are assumed to be a mixture of fuel, air, and inert gases. The composition of the residuals is determined based on the stoichiometry of the prior cycle to establish the fraction of the inert from both EGR and combustion. The NNs were

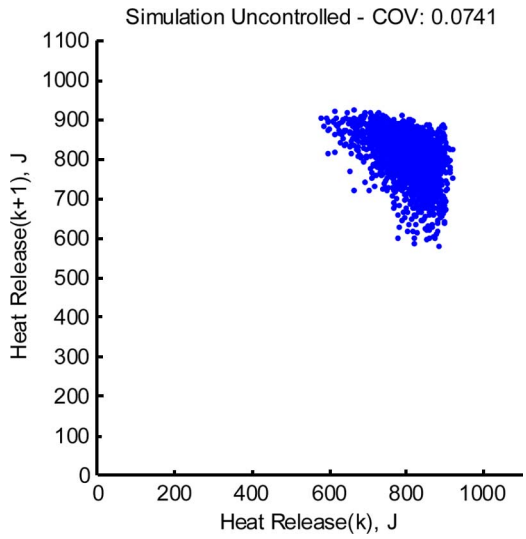

Fig. 2. Heat release return map without control (24% EGR).

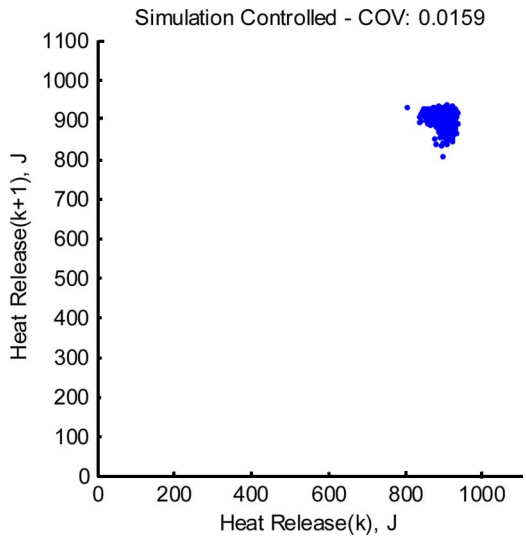

Fig. 3. Heat release return map with control (24% EGR).

designed to have 15 neurons each in the hidden layer with learning rates of 0.01 each so that (71) is satisfied. Here, the heat release value is normalized.

The activation functions used were the hyperbolic tangent sigmoid functions. Simulations ran for 1000 cycles of engine operation at each EGR value ranging from 19% to 24%. The attached plots show the results obtained from the simulation runs at EGR levels of 24%. The dispersion of heat release in the return map of Fig. 3 is less than that seen in Fig. 2, according to the lower COV which has reduced from 0.0741 to 0.0159.

The COV metric—hereafter referred to as COV—is used to quantify cyclic dispersion due to heat release. It is calculated as the standard deviation of a set of heat release data divided by the mean heat release for that set. A larger COV indicates that heat release values were more dispersed on the return map. With regard to COV, a goal for this controller implementation is to observe a reduction in COV when the control loop is closed on the engine.

The COV in integrated cycle work is often used to establish variability in engine output. With the integrated cycle work obtained from the cyclic cylinder pressure–volume results, the COV is obtained by dividing the standard deviation in cycle work by the mean over all of the cycles observed. It was observed that with the NN applied, the engine model exhibits minimal dispersion with high EGR levels even with perturbation on the residual gas fraction being unknown. The reduction in dispersion physically translates into fewer partial burning cycles even with high EGR levels in the engine.

Although exhibiting very similar dynamics, the return maps of heat release are quantitatively different between the simplified model used for controller development and testing and the actual engine as presented in the following. This can be attributed to the fact that the engine model simply considers mass conservation of the fuel, air, and combustion product species and places all complexities of the fluid mechanics and combustion into a phenomenological nonlinear combustion efficiency term and stochastic variations. In spite of this simplicity in the model, the designed controller performs highly satisfactorily on the actual engine as will be seen in the following.

VI. Controller Hardware Design

The experimental setup involves two research engines. The first is a CFR engine and the second is a Ricardo hydra engine with a modern four-valve Ford Zetec head. Both engines are operated at 1000 r/min while multiple load set points are tested through the addition of diluent. Being single cylinder engines, dynamics introduced by multiple cylinders are avoided.

For each engine, shaft encoders are mounted on the cam and crank shafts that return start-of-cycle and crank angle signals, respectively. There are 720° of crank angle per engine cycle, so a crank angle degree is detected every 167 μs at this engine speed. For the EGR portion of gaseous intake, nitrogen is used. EGR is comprised mainly of inert gases from the previous combustion cycle, so nitrogen, an inert gas in the combustion process, is used in place of the residual inert gases. This allows for accurate metering of an average EGR flow to the cylinder.

Heat release for a given engine cycle is calculated by integrating in-cylinder pressure and volume over time. In-cylinder pressure is measured every half crank angle degree during combustion, which is considered from 345° to 490°, for a total of 290 pressure measurements. At 1000-r/min pressure measurements must be made every 83.3 μs. The calculation window is 106° wide or 17.667 ms. At this time, all engine-to-PC-to-engine communications are completed. The algorithm designed uses 15 neurons to approximate the output, though it can be seen from Fig. 5 that even at 100 controller nodes and 100 observer nodes calculations are complete within 1.2 ms, well within the available time of 17.667 ms.

Since the number of nodes required in a multilayer NN for a given approximation error is not clear in the literature, the plot in Fig. 4 illustrates that even with large number of hidden-layer NNs the proposed controller can be implemented on the embedded hardware. However, it was found from offline analysis that the improvement in approximation accuracy is not significant beyond 15 hidden-layer nodes and, therefore, the hidden-layer NN nodes in the observer and controller are limited to 15.

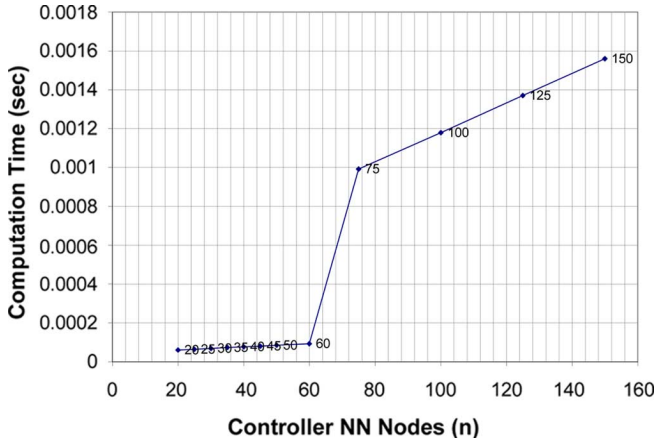

Fig. 4. NN controller runtimes varying nodes.

TABLE I
COV FOR CFR

EGR	Uncontrolled COV	Controlled COV
5%	0.0873	0.0347
10%	0.1873	0.0838

The control input is an adjustment to the nominal fuel required at a given equivalence ratio. Fuel injection is controlled by a transistor–transistor logic (TTL) signal to a fuel injector driver circuit. Pressure measurements come from a charge amplifier which receives pressure transducer signals from a piezoelectric transducer located inside the cylinder.

An engine-to-PC interface board was designed to manage the shaft encoder signals, pressure measurements, and fuel injector signal since timing is crucial to correct engine operation. The board uses a microcontroller to communicate between the TTL and analog signals of the engine hardware and a parallel digital input–output (I/O) port of the PC. A high-speed, 8-b, analog-to-digital (A/D) converter converts the pressure measurements. Pressure measurements are sent to the PC where heat release is calculated before being sent to the controller. Fuel pulse width for the next engine cycle is sent to the microcontroller from the PC.

VII. EXPERIMENTAL RESULTS

The results for engine operation at a near-stoichiometric equivalence ratio and addition of a percentage of EGR to the contents of the cylinder are discussed. Equation (75) shows how the mass of nitrogen m_{EGR} is chosen to give a desired percentage of EGR

$$\%\mathrm{EGR} = 100 \times \left(\frac{m_{\mathrm{EGR}}}{m_f + m_a + m_{\mathrm{EGR}}} \right). \tag{75}$$

As mentioned in Section V, COV is a metric that can quantify a reduction in cyclic dispersion when viewing a return map. The following return maps for the two engines on which the controller was operated have COV information. It is shown that with control, the COV is reduced. Again, this reduction in COV means that the engine is more stable in the presence of high intake EGR.

Typically, COV values less than 10% are considered acceptable for production engines. The ideal COV would be 0%. More realistically, the cyclic dispersion of an engine cannot be reduced to less than the case where equivalence ratio is stoichiometric and no EGR is present due to ever present stochastic effects. The experimental results will show that the controller can reduce the cyclic dispersion, measured as a reduction in the COV metric.

Figs. 5–11 are results from engine controller tests on the CFR engine. The uncontrolled engine equivalence ratio was near-stoichiometric at 0.97. The controller pushed the equivalence ratio to 1.0, due to the behavior of the control input $u(k)$. Equivalence ratios experienced for both uncontrolled and controlled scenarios are near-stoichiometric although the control input $u(k)$ slightly modifies the effective equivalence ratio over time.

Heat release time series and return maps were generated for both controlled and uncontrolled cases for each of three EGR set points: 0%, 5%, and 10%. These EGR values correspond to average IMEP load values of 528, 476, and 410 kPa, respectively. Before engine tests, air flow is measured and nominal fuel is calculated for the desired equivalence ratio. The nominal fuel and air are loaded into the controller configuration. During data acquisition, ambient pressure is referenced in the acquired cylinder pressure each engine cycle based on the in-cylinder pressure when the exhaust valve is fully open at 600°.

The NN weight values are all initialized at zero. Heat release return maps in Figs. 5 and 6 depict the performance of the proposed NN controller for the 0% EGR case. It is important to observe that the return maps of heat release with no control are slightly below the target value whereas with the application of control the heat release return maps are around the target value. Moreover, no misfire is noted. Figs. 7 and 8 show a decrease in cyclic dispersion for 5% EGR which corroborates the results seen in simulation. During the absence of control, there is much cyclic dispersion and occasional misfires, and during control the misfires and dispersion are reduced.

The return maps at 10% EGR show distinct cyclic dispersion during no control and a significant decrease in those dispersed data points during control.

It can be seen that the mean heat release increases with control, which corresponds to a slightly higher equivalence ratio. The equivalence ratio for EGR operation is intended to be held fixed at 1.00. When using fuel as the control input, the controller must change the fuel to affect the engine, and therefore, changes the equivalence ratio. Fuel intake increases slightly during control causing the actual operating equivalence ratio to be slightly higher than the set point, here, at 1.0. It is thought that this is partly due to a higher value specified for target heat release compared to uncontrolled case. Moreover, this slight offset remains due to slow learning of the NNs which eventually becomes zero with time. A tradeoff exists between speed of learning and performance. Higher learning rate for NNs slightly degrades performance in terms of dispersion and vice versa.

The COV for the EGR return maps is listed in Table I for the CFR engine. As the EGR percentage of cylinder

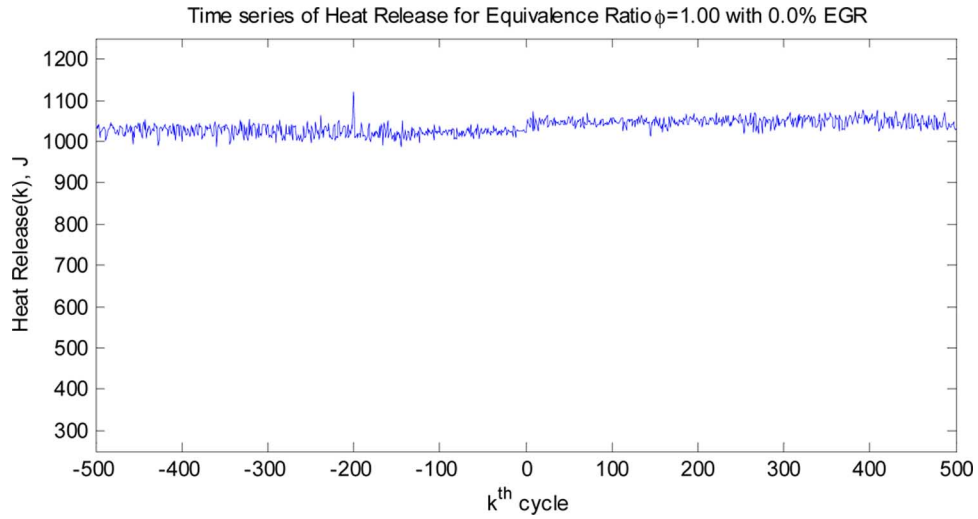

Fig. 5. CFR engine heat release (in joules) time series at 0% EGR.

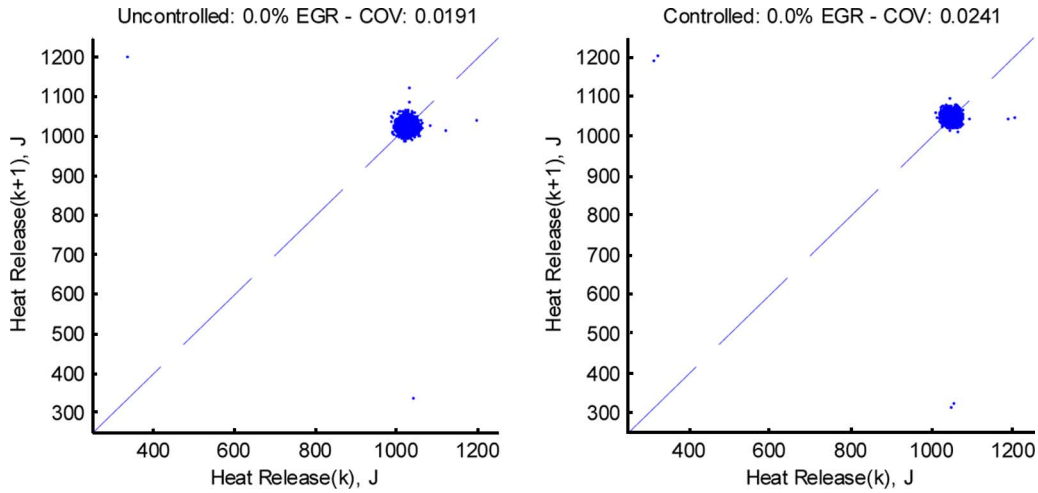

Fig. 6. Uncontrolled and controlled heat release return maps plotting current cycle $y(k)$ against next cycle $y(k+1)$ at 0% EGR on CFR engine.

contents is increased from 0% to 10%, the COV increases for uncontrolled engine operation. The increased COV indicates increased cyclic dispersion as seen in the uncontrolled EGR return maps. The COV decreases when control is applied in the presence of EGR, a decrease of 55% at 10% EGR, meaning the controller has made the engine more stable. Consequently, a 25% drop in uHC is observed with 10% EGR for this engine. Additionally, 80% drop in NO_x from stoichiometric levels is noted.

Figs. 11–18 are data collected from engine controller operation on the Ricardo research engine. Performance of the controller was similar in that decreases in cyclic dispersion for high EGR cases were seen. Higher EGR is possible with the Ricardo engine because it is a faster burning engine, and hence, it is more tolerant of diluent addition. The fuel control input does not increase as much on the Ricardo engine as with the CFR engine, so the time series of heat release plots do not exhibit increase when control is activated. Total fuel input during control was not more than 1.5% from the nominal fuel for the desired stoichiometric equivalence ratio.

Aside from the stoichiometric operating condition with no EGR added to the Ricardo engine, three cases of high EGR were tested. EGR levels of 0%, 12.9%, 15.2%, and 18.5% were used to obtain data. These values correspond to IMEP load values of 881, 716, 594, and 297 kPa, respectively.

In Fig. 11, the time series of heat release is plotted, showing the last 500 cycles of the uncontrolled data set with the transition to the first 500 cycles of data with the controller enabled. As seen in Fig. 12, there is very little cyclic dispersion at this stoichiometric case without EGR present, indicated by the low COV value of 2.6%. This set point can be considered optimal in that the engine is operating under ideal conditions. When the controller is enabled, very little improvement can be made to reduce the stochastic dispersion beyond the engine's most stable operating point.

In Figs. 13 and 14, the effect of about 12.9% EGR causes the engine to become less stable. The controller causes a reduction in cyclic dispersion by comparing the COV values for uncontrolled and controlled data in Fig. 14. The COV falls from 0.0462 to 0.0352.

One can see from Figs. 17 and 18 that 15.2% EGR causes the engine to become much more unstable than for the case of 12.9% EGR. The controller yields a significant improvement, reducing the dispersion by 33% from 0.1345 to 0.0891.

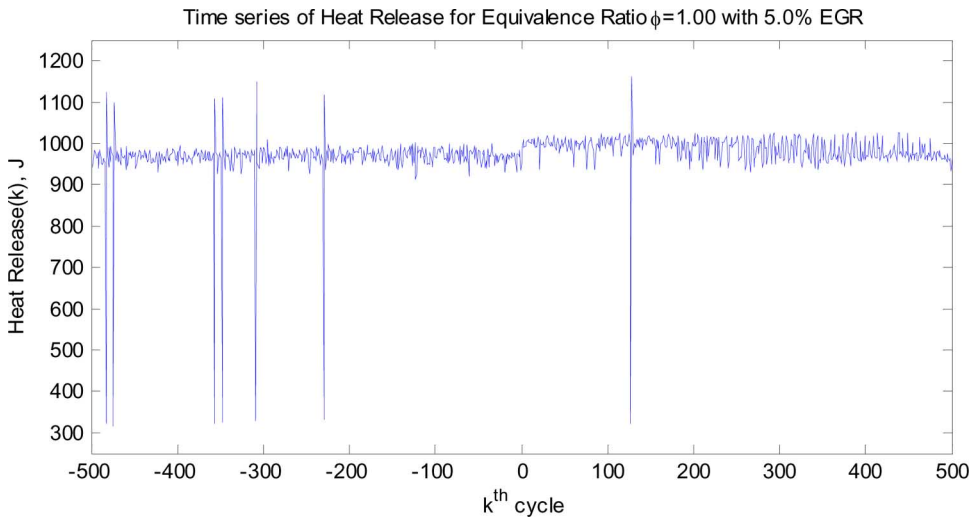

Fig. 7. CFR engine heat release time series at 5% EGR.

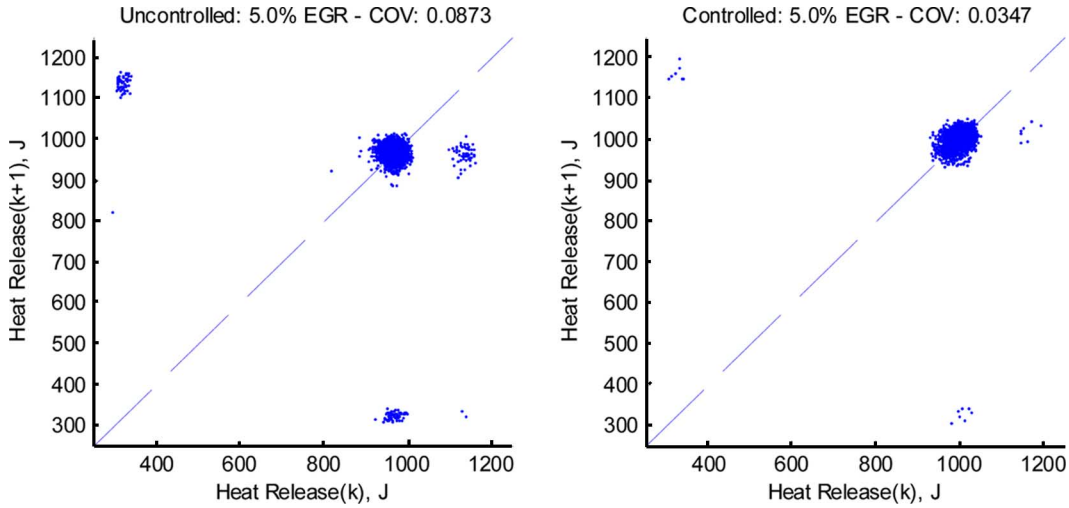

Fig. 8. Uncontrolled and controlled heat release return maps plotting current cycle $y(k)$ against next cycle $y(k+1)$ at 5% EGR on CFR engine.

In Figs. 17 and 18, a case of very high EGR is shown for the Ricardo engine. At 18.5% EGR, the engine becomes very unstable, exhibiting significant cyclic dispersion of heat release. However, the controller is still able to reduce dispersion from 0.3733 to 0.3419.

The COV values for the Ricardo engine data are shown in Table II. The controller reduces COV for every case, corresponding to a decrease in cyclic dispersion. Hence, the controller can make the engine more stable in the presence of high EGR.

The engine-out emissions of uHC and NO_x for the Ricardo engine are shown in Table III. Prefixes of "u" and "c" given before the emission type represent uncontrolled and controlled, respectively. For all cases of EGR, uHC diminish with the controller enabled. This can be expected since the controller is reducing the number of partial burns encountered in the heat release. Table data for NO_x shows a significant reduction at high levels of EGR. The controller makes engine operation more stable which increases the mean heat release. The higher burn temperatures within the cylinder during control cause the NO_x to slightly increase when the controller is activated compared to without control. At 15% EGR, a drop of 90% NO_x from stoichiometric levels is observed. At this EGR level, an improvement in fuel conversion efficiency of 2% is also noted. This improvement is the direct result of reduced cyclic dispersion. Even further improvement in fuel efficiency should be possible with further reduction in dispersion as this control scheme is refined.

Results from the controller implementation on two different engines exemplify the controller's flexibility. Only engine parameters such as fuel injector information and cylinder geometry had to be changed to extend the controller from the CFR engine to the Ricardo engine. No offline NN training is required and the controller is model-free. Finally, the task of identifying stabilizing initial weights for the observer and controller NNs, a well-known problem in the literature [19], is overcome by initializing the NN weights to zero.

VIII. Conclusion

A novel NN controller scheme is presented to reduce the cyclic dispersion in heat release at high EGR levels for an SI

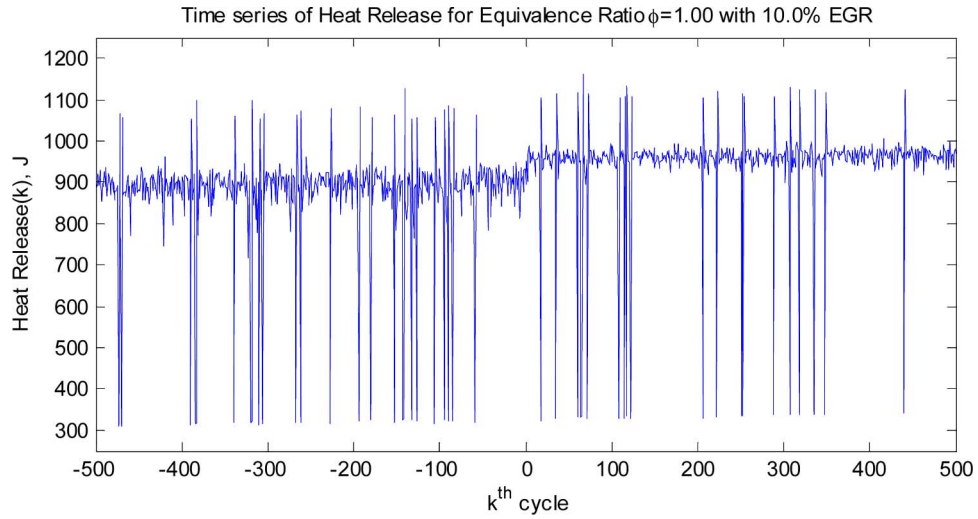

Fig. 9. CFR engine heat release time series at 10% EGR.

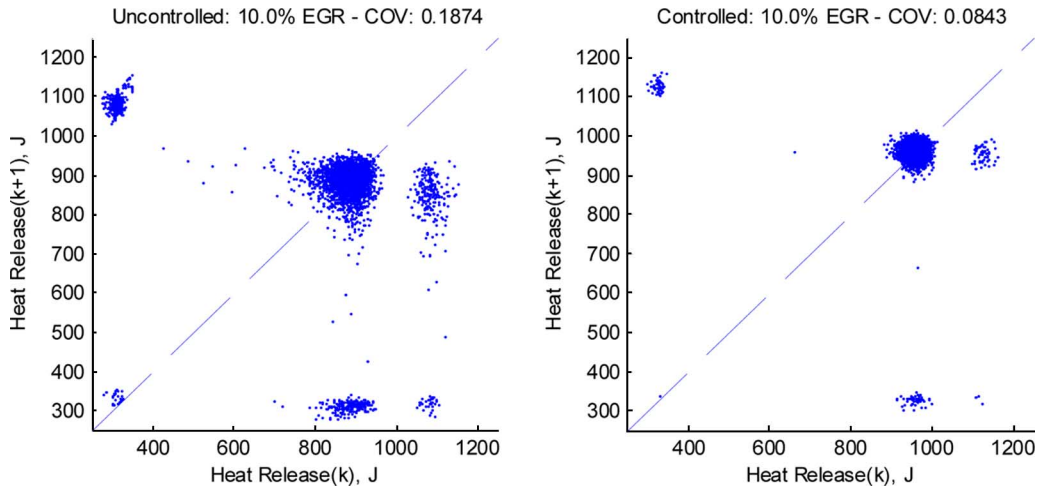

Fig. 10. Uncontrolled and controlled heat release return maps plotting current cycle $y(k)$ against next cycle $y(k+1)$ at 10% EGR on CFR engine.

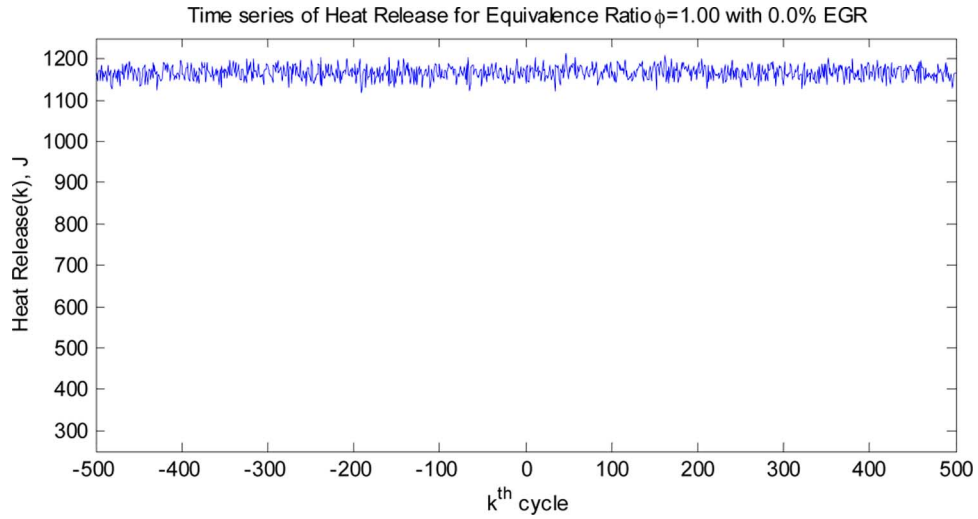

Fig. 11. Ricardo engine heat release time series at 0% EGR.

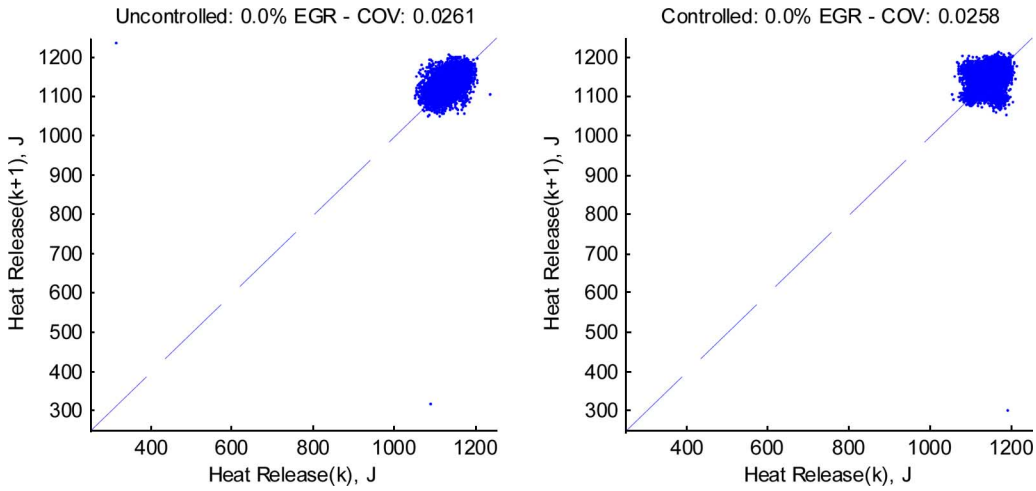

Fig. 12. Uncontrolled and controlled heat release return maps plotting current cycle $y(k)$ against next cycle $y(k+1)$ at 0% EGR on Ricardo.

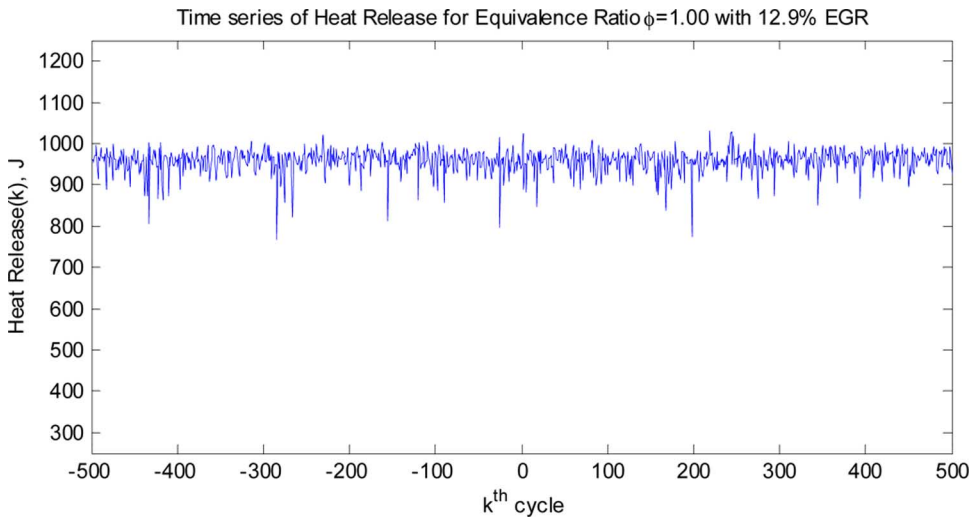

Fig. 13. Ricardo engine heat release time series at 12.9% EGR for Ricardo.

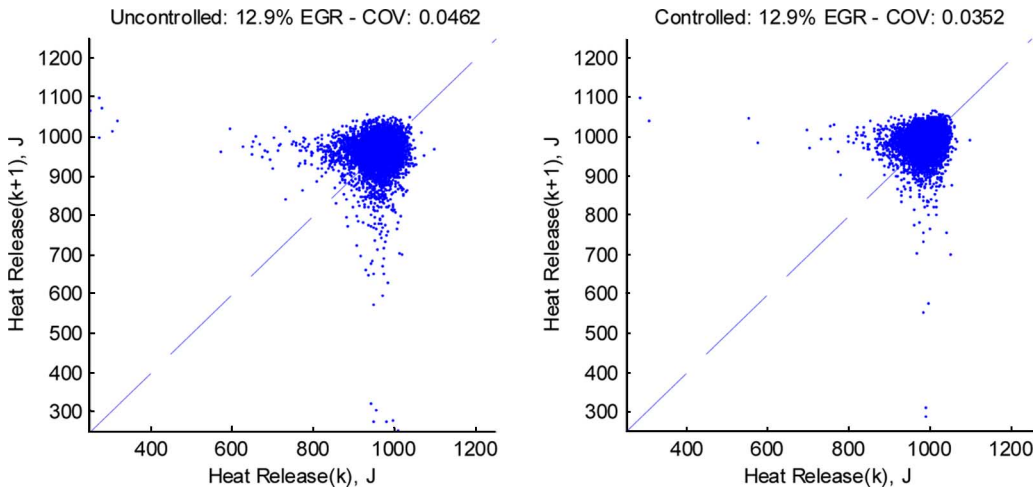

Fig. 14. Uncontrolled and controlled heat release return maps plotting current cycle $y(k)$ against next cycle $y(k+1)$ at 12.9% EGR on Ricardo.

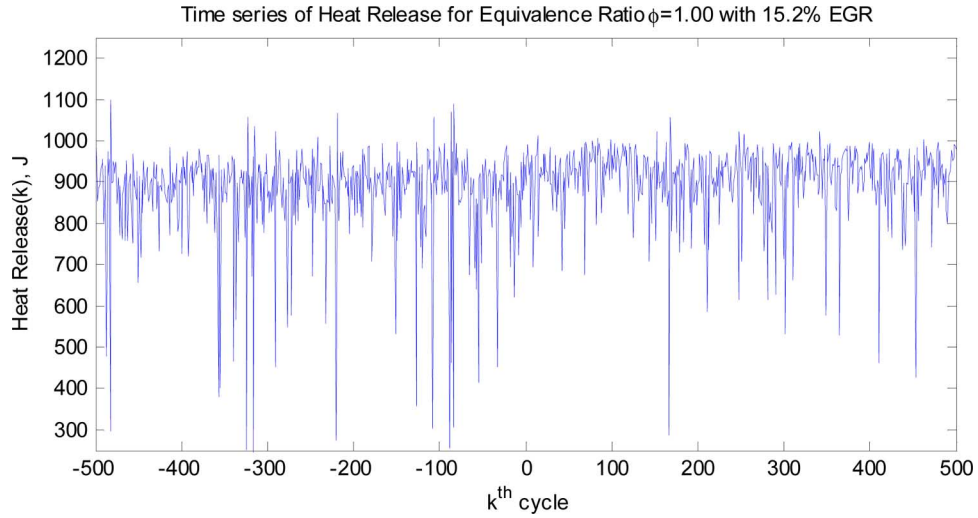

Fig. 15. Ricardo engine heat release time series at 15.2% EGR for Ricardo.

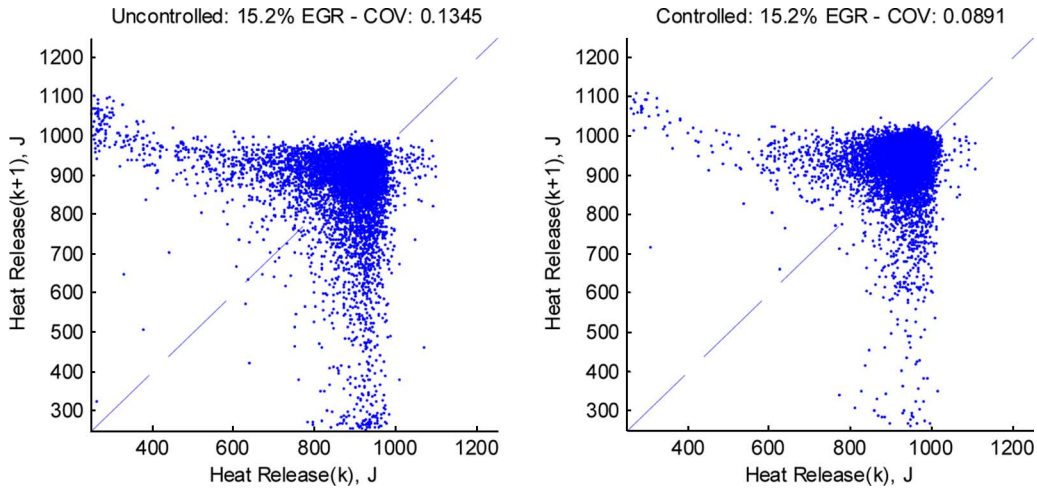

Fig. 16. Uncontrolled and controlled heat release return maps plotting current cycle $y(k)$ against next cycle $y(k+1)$ at 15.2% EGR on Ricardo.

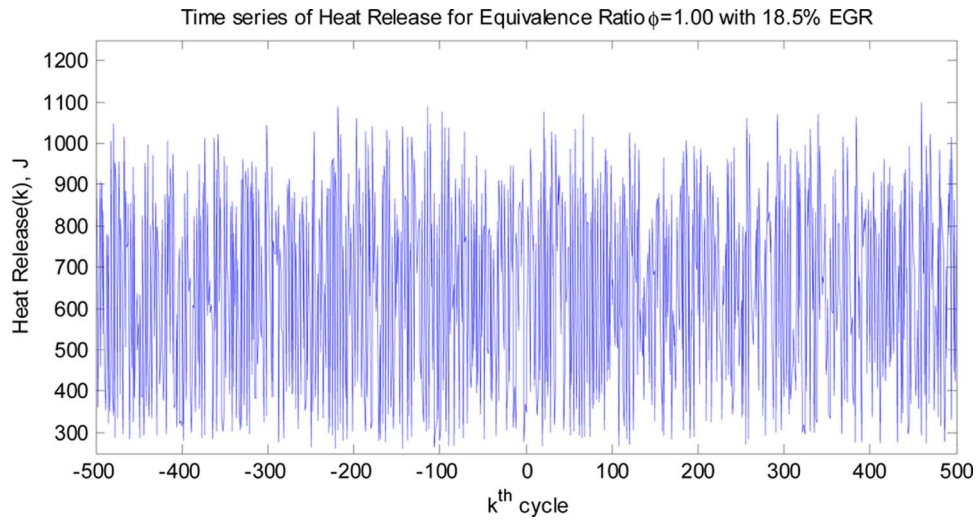

Fig. 17. Ricardo engine heat release time series at 18.5% EGR for Ricardo.

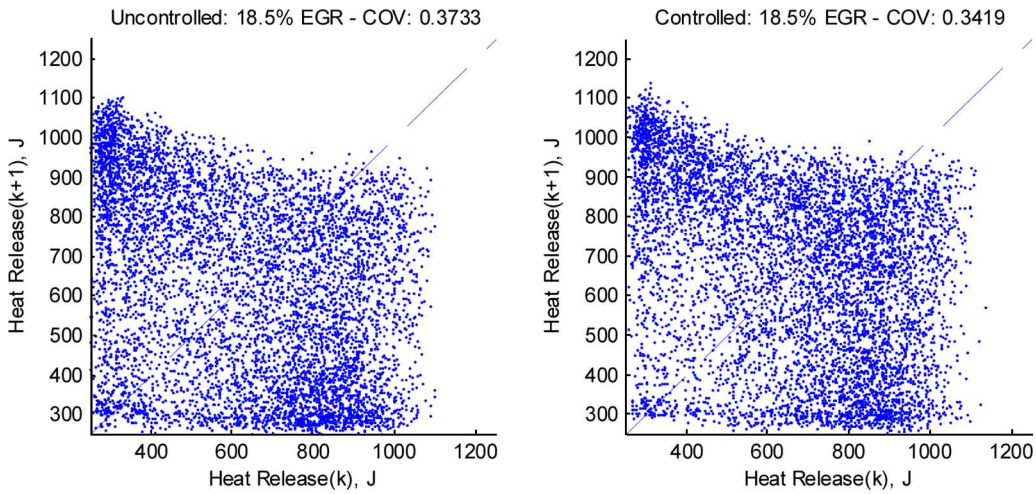

Fig. 18. Uncontrolled and controlled heat release return maps plotting current cycle $y(k)$ against next cycle $y(k+1)$ at 18.5% EGR on Ricardo.

TABLE II
COV FOR RICARDO

EGR	Uncontrolled COV	Controlled COV
0.0%	0.0261	0.0258
12.9%	0.0462	0.0352
15.2%	0.1345	0.0891
18.5%	0.3733	0.3419

TABLE III
EGR NO_x AND UHC EMISSIONS DATA FOR RICARDO

EGR	(u) NO_x (PPM)	(c) NO_x (PPM)	(u) uHC (PPM)	(c) uHC (PPM)
0.0%	5443	4995	3399	3532
12.9%	572	628	3905	3825
15.2%	204	306	4420	4162
18.5%	43	50	10370	9051

engine which is modeled as a nonstrict feedback nonlinear discrete-time system. The proposed control scheme utilizes both the NN approximation property and a backstepping-type approach for maintaining a fixed A/F ratio by altering the fuel injected into the cylinder as the control input. The stability analysis of the closed-loop control system was conducted and the boundedness of the closed-loop signals was shown.

Experimental results show that the performance of the proposed controller is highly satisfactory while meeting the closed-loop stability even though the dynamics are not known beforehand. Using the nonlinear backstepping-like controller, the cyclic dispersion could be reduced significantly, resulting in the potential for decreased emissions and improved fuel economy. Even though the controller was designed for the model heat release output which does not exhibit all the nonlinearities of actual engine heat release, the controller was still able to minimize heat release error. Persistency of excitation condition is not needed, separation principle and certainty equivalence principle are relaxed, and linear in the unknown parameter assumption is not used.

Experimental results indicate that the controller can improve engine stability and reduce uHC at high levels of EGR where significant reductions in NO_x can be realized. Furthermore, the controller is flexible enough to be implemented on two SI research engines.

APPENDIX

Proof of Theorem: Define the Lyapunov function

$$J(k)=\sum_{i=1}^{3}\frac{\gamma_i}{\alpha_i}\tilde{w}_i^T(k)\tilde{w}_i(k)+\frac{\gamma_4}{\alpha_4}\tilde{x}_1^2(k)+\frac{\gamma_5}{5}\tilde{x}_2^2(k)+\frac{\gamma_6}{3}\tilde{y}^2(k)+\frac{\gamma_7}{3}e_1^2(k)+\frac{\gamma_8}{4}e_2^2(k) \quad \text{(A.1)}$$

where $0<\gamma_i$, $i=1,5,8$, are auxiliary constants, the NN weights estimation errors $\tilde{w}_1$, $\tilde{w}_2$, and $\tilde{w}_3$ are defined in (36), (46), and (63), respectively, the observation errors $\tilde{x}_1(k)$, $\tilde{x}_2(k)$, and $\tilde{y}(k)$ are defined in (32) and (29), the system errors $e_1(k)$ and $e_2(k)$ are defined in (38) and (47), respectively, and α_i, $i=1,2,3$, are NN adaptation gains. The Lyapunov function (A.1) consisting of the system errors, observation errors, and the weights estimation errors obviates the need for separation principle and certainty equivalence principle (CE).

The first difference of Lyapunov function is given by

$$\Delta J(k)=\sum_{i=1}^{8}\Delta J_i(k). \quad \text{(A.2)}$$

The first term of $\Delta J_1(k)$ is obtained by using (68) as

$$\begin{aligned}\Delta J_1(k)&=\frac{\gamma_1}{\alpha_1}\left[\tilde{w}_1^T(k+1)\tilde{w}_1(k+1)-\tilde{w}_1^T(k)\tilde{w}_1(k)\right]\\&\le-\gamma_1\left(1-\alpha_1\|\phi_1(\cdot)\|^2\right)\left(\hat{w}_1^T(k)\phi_1(\cdot)+l_5\tilde{y}(k)\right)^2\\&\quad-\gamma_1\zeta_1^2(k)+2\gamma_1 l_5^2\tilde{y}^2(k)+2\gamma_1\left(w_1^T\phi_1(\cdot)\right)^2 \quad \text{(A.3)}\end{aligned}$$

where $\zeta_1(k)$ is defined in (37).

Now, taking the second term in the first difference (A.1) and substituting (69) into (A.2), we get

$$\begin{aligned}\Delta J_2(k) &= \frac{\gamma_2}{\alpha_2}\left[\tilde{w}_2^T(k+1)\tilde{w}_2(k+1) - \tilde{w}_2^T(k)\tilde{w}_2(k)\right] \\ &\le -\gamma_1\left(1-\alpha_2\left\|\phi_2(\cdot)\right\|^2\right) \\ &\quad\times\left(\hat{w}_2^T(k)\phi_2(\cdot) + l_6\tilde{x}_1(k) + l_6 e_1(k)\right)^2 - \gamma_2\zeta_2^2(k) \\ &\quad + 3\gamma_2 l_6^2\tilde{x}_1^2(k) + 3\gamma_2 l_6^2 e_1^2(k) \\ &\quad + 3\gamma_2\left(w_2^T\phi_2(\cdot)\right)^2. \end{aligned} \tag{A.4}$$

Taking the third term in the first difference (A.1) and substituting (70) into (A.2), we get

$$\begin{aligned}\Delta J_3(k) &= \frac{\gamma_3}{\alpha_3}\left[\tilde{w}_3^T(k+1)\tilde{w}_3(k+1) - \tilde{w}_3^T(k)\tilde{w}_3(k)\right] \\ &\le -\gamma_3\left(1-\alpha_3\left\|\phi_3(\cdot)\right\|^2\right) \\ &\quad\times\left(\hat{w}_3^T(k)\phi_3(\cdot) + l_7\tilde{x}_2(k) + l_7 e_2(k)\right)^2 - \gamma_3\zeta_3^2(k) \\ &\quad + 3\gamma_2 l_7^2\tilde{x}_2^2(k) + 3\gamma_3 l_7^2 e_1^2(k) \\ &\quad + 3\gamma_3\left(w_3^T\phi_3(\cdot)\right)^2. \end{aligned} \tag{A.5}$$

Similarly, we have

$$\begin{aligned}\Delta J_4(k) \le{}& \gamma_4\left[F_o^2\tilde{x}_1^2(k) + (l_2 - R\cdot F_o)^2\tilde{y}^2(k) + \Delta F^2(k)e_1^2(k)\right] \\ &+ \gamma_4\Big[l_1'(k))^2 e_2^2(k) + l_1'(k))^2\zeta_2^2(k) \\ &\quad + d_{11}^2(k) - \tilde{x}_1^2(k)\Big] \end{aligned} \tag{A.6}$$

where

$$l_1'(k) = R\cdot\Delta F(k).\mathrm{CE}(k) \tag{A.7}$$

$$\begin{aligned} d_{11} &= R\cdot\Delta F(k).\mathrm{CE}(k).w_2^T\phi_2(\cdot) - \Delta x_{1\mathrm{new}}(k) - d_1(k) \\ &\quad - (\Delta F + F_o)\left(r_{\mathrm{O}_2} + r_{\mathrm{N}_2}\right) \end{aligned} \tag{A.8}$$

and $\zeta_2(k)$ is defined in (51)

$$\begin{aligned}\Delta J_5(k) ={}& \gamma_5\left[F_o^T\tilde{x}_2^2(k) + (l_2 - F_o)^2\tilde{y}^2(k) + d_{21}^2(k) - \tilde{x}_2^2(k)\right] \\ &+\gamma_5\left[\left((1-\mathrm{CE}(k)\Delta F(k))^2\left(e_2^2(k) + \zeta_2^2(k)\right)\right)\right] \end{aligned} \tag{A.9}$$

where

$$d_{21} = -d_2(k) - \Delta F(k)\left(1-\mathrm{CE}(k)\right)\cdot w_2^T\phi_2(\cdot) \tag{A.10}$$

$$\Delta J_6(k) \le \gamma_6\left(\zeta_1^2(k) + l_3^2\tilde{y}^2(k) + d_3^2(k) - \tilde{y}^2(k)\right) \tag{A.11}$$

$$\Delta J_7(k) \le \gamma_7\left(g_1^2(k)g_2^2(k) + g_1^2\zeta_1^2(k) + d_{12}^2(k) - e_1^2(k)\right) \tag{A.12}$$

$$\Delta J_8(k) \le \gamma_8\left(l_4^2(k)e_2^2(k) + l_4^2\tilde{x}_2^2(k) + \zeta_3^2(k) + d_{22}^2(k) - e_2^2(k)\right). \tag{A.13}$$

Combining (A.3)–(A.13) to get the first difference of the Lyapunov function and simplifying it, we get

$$\begin{aligned}\Delta J(k) \le{}& -\gamma_1\left(1-\alpha_1\left\|\phi_1(\cdot)\right\|^2\right)\left(\hat{w}_1^T(k)\phi_1(\cdot) + l_5\tilde{y}(k)\right)^2 \\ &+ l_6\tilde{x}_1(k) - \gamma_2\left(1-\alpha_2\left\|\phi_2(\cdot)\right\|^2\right) \\ &\times\left(\hat{w}_2^T(k)\phi_2(\cdot) + l_6 e_1(k)\right)^2 + l_7\tilde{x}_2(k) \\ &- \gamma_3\left(1-\alpha_3\left\|\phi_3(\cdot)\right\|^2\right)\left(\hat{w}_3^T(k)\phi_3(\cdot) - (\gamma_1 - \gamma_6)\right. \\ &\times\zeta_1^2(k) - \left(\gamma_2 - \gamma_4\left(l_1'(k)\right)^2 + l_7 e_2(k)\right)^2 \\ &- \gamma_5\left(\left(1-\mathrm{CE}(k)\Delta F(k)\right)^2 - \gamma_7 g_1^2(k)\right)\zeta_2^2(k) \\ &- (\gamma_2 - \gamma_4)\zeta_3^2(k) - \left(\left(1-F_o^2\right)\gamma_4 - 3\gamma_2 l_6^2\right)\tilde{x}_1^2(k) \\ &- \left(\left(1-F_o^2\right)\gamma_5 - 3\gamma_3 l_7^2 - \gamma_8 l_4^2\right)\tilde{x}_2^2(k) \\ &- \left(\left(1-l_3^2\right)\gamma_6 - (l_1 - R\cdot F_o)^2\gamma_4\right. \\ &\quad -(l_2 - F_o)^2\gamma_5 - 2\gamma_1 l_5^2\big)\tilde{y}^2(k) \\ &- \left(\gamma_7 - 3\gamma_2 l_6^2 - \gamma_4\Delta F^2(k)\right)e_1^2(k) \\ &- \left(\left(1-l_4^2\right)\gamma_8 - 3\gamma_3 l_7^2 - \gamma_4\left(l_7'(k)\right)^2\right. \\ &\quad - \gamma_7 g_1^2(k)e_2^2(k) - \gamma_5\Big(\left(1-\mathrm{CE}(k)\Delta F(k)\right)^2 \\ &+ D_M^2 \end{aligned} \tag{A.14}$$

where

$$\begin{aligned} D_M^2 = {}& 2\gamma_1 w_{1m}^2\phi_{1m}^2 + 3\gamma_2 w_{2m}^2\phi_{2m}^2 + 3\gamma_3 w_{3m}^2\phi_{3m}^2 + \gamma_4 d_{11m}^2 \\ &+\gamma_5 d_{21m}^2 + \gamma_6 d_{3m}^2 + \gamma_7 d_{12m}^2 + \gamma_8 d_{22m}^2. \end{aligned} \tag{A.15}$$

Choose $\gamma_1 = 2$, $\gamma_2 = 1$, $\gamma_3 = 3$, $\gamma_4 = (1/6R^2\Delta F_m^2)$, $\gamma_5 = (1/6\Delta F_m^2)$, $\gamma_6 = 1$, $\gamma_7 = (1/3R^2)$, and $\gamma_8 = 1$; then, (A.14) is simplified as

$$\begin{aligned}\Delta J(k) \le{}& -2\left(1-\alpha_1\left\|\phi_1(\cdot)\right\|^2\right)\left(\hat{w}_1^T(k)\phi_1(\cdot) + l_5\tilde{y}(k)\right)^2 \\ &-\left(1-\alpha_2\left\|\phi_2(\cdot)\right\|^2\right) \\ &\times\left(\hat{w}_2^T(k)\phi_2(\cdot) + l_6\tilde{x}_1(k) + l_6 e_1(k)\right)^2 \\ &-2\left(1-\alpha_3\left\|\phi_3(\cdot)\right\|^2\right) \\ &\times\left(\hat{w}_3^T(k)\phi_3(\cdot) + l_7\tilde{x}_2(k) + l_7 e_2(k)\right)^2 - \zeta_1^2(k) \\ &-\frac{1}{3}\zeta_2^2(k) - \zeta_3^2(k) - \left(\frac{\left(1-F_o^2\right)}{6R^2\Delta F_m^2} - 3l_6^2\right)\tilde{x}_1^2(k) \\ &-\left(\frac{\left(1-F_o^2\right)}{6\Delta F_m^2} - 6l_7^2 - l_4^2\right)\tilde{x}_2^2(k) \\ &-\left(\left(1-l_3^2\right) - \frac{(l_1 - R\cdot F_o)^2}{6R^2\Delta F_m^2}\right. \\ &\quad -\frac{(l_2 - F_o)^2}{6\Delta F_m^2} - 4l_5^2\Big)\tilde{y}^2(k) \\ &-\left(\frac{1}{6R^2} - 3l_6^2\right)e_1^2(k) + D_M^2 \\ &-\left(\left(1-l_4^2\right) - 6l_7^2 - \frac{2}{3}\right)e_2^2(k). \end{aligned} \tag{A.16}$$

This implies $\Delta J(k) < 0$ as long as (70)–(72) hold and

$$|\zeta_1(k)| > D_M \quad \text{or} \quad |\zeta_2(k)| > \sqrt{3}D_M \quad \text{or} \quad |\zeta_3(k)| > D_M \tag{A.17}$$

or

$$|\tilde{x}_1(k)| > \frac{D_M}{\sqrt{\frac{(1-F_o^2)}{6R^2\Delta F_m^2} - 3l_6^2}}$$

or

$$|\tilde{x}_2(k)| > \frac{D_M}{\sqrt{\frac{(1-F_o^2)}{6\Delta F_m^2} - 6l_7^2 - l_4^2}} \tag{A.18}$$

or

$$|\tilde{y}(k)| > \frac{D_M}{\sqrt{(1-l_3^2) - \frac{(l_1 - R\cdot F_o)^2}{6R^2\Delta F_m^2} - \frac{(l_2 - F_o)^2}{6\Delta F_m^2} - 4l_5^2}} \tag{A.19}$$

or

$$|e_1(k)| > \frac{D_M}{\sqrt{\frac{1}{6R^2} - 3l_6^2}} \quad |e_2(k)| > \frac{D_M}{\sqrt{\left(\frac{1}{3} - l_4^2\right) - 6l_7^2}}. \tag{A.20}$$

According to a standard Lyapunov extension theorem [17], [19], this demonstrates that the system tracking error and the weight estimation errors are UUB. The boundedness of $\|\zeta_1(k)\|$, $\|\zeta_2(k)\|$, and $\|\zeta_3(k)\|$ implies that the weight estimation errors $\|\tilde{w}_1(k)\|$, $\|\tilde{w}_2(k)\|$, and $\|\tilde{w}_3(k)\|$ are bounded, and this further implies that the weight estimates $\|\hat{w}_1(k)\|$, $\|\hat{w}_2(k)\|$, and $\|\hat{w}_3(k)\|$ are bounded. Therefore, all the signals in the closed-loop system are bounded.

REFERENCES

[1] K. P. Dudek and M. K. Sain, "A control-oriented model for cylinder pressure in internal combustion engines," *IEEE Trans. Autom. Control*, vol. 34, no. 4, pp. 386–397, Apr. 1989.

[2] R. W. Sutton and J. A. Drallmeier, "Development of nonlinear cyclic dispersion in spark ignition engines under the influence of high levels of EGR," in *Proc. Central States Section Combustion Inst.*, Indianapolis, IN, Apr. 16–18, 2000, pp. 175–180, 2000.

[3] P. He and S. Jagannathan, "Neuroemission controller for reducing cyclic dispersion in lean combustion spark ignition engines," *Automatica*, vol. 41, pp. 1133–1142, April 2005.

[4] C. S. Daw, C. E. A. Finney, M. B. Kennel, and F. T. Connolly, "Observing and modeling nonlinear dynamics in an internal combustion engine," *Phys. Rev. E, Stat. Phys. Plasmas Fluids Relat. Interdiscip. Top.*, vol. 57, no. 3, pp. 2811–2819, 1998.

[5] C. S. Daw, C. E. A. Finney, J. B. Green, M. B. Kennel, and J. F. Thomas, "A simple model for cyclic variations in a spark-ignition engine," *Soc. Automotive Engineers*, ser. Tech. Papers, May 1996, 962086.

[6] J. B. Heywood, *Internal Combustion Engine Fundamentals*. New York: MGraw-Hill, 1998.

[7] T. Inoue, S. Matsushita, K. Nakanishi, and H. Okano, "Toyota lean combustion system—The third generation system," *Soc. Automotive Engineers*, ser. Tech. Papers, 1993, 930873.

[8] R. M. Wagner, "Identification and characterization of complex dynamic structure in spark ignition engines," Ph.D. dissertation, Dept. Mech. Eng., Univ. Missouri-Rolla, Rolla, MO, 1999.

[9] R. M. Wagner, J. A. Drallmeier, and C. S. Daw, "Nonlinear cycle dynamics in lean spark ignition combustion," in *Proc. 27th Int. Symp. Combustion, The Combustion Inst.*, 1998, pp. 2127–2133.

[10] P. C. Yeh and P. V. Kokotovic, "Adaptive output feedback design for a class of nonlinear discrete-time systems," *IEEE Trans. Autom. Control*, vol. 40, no. 9, pp. 1663–1668, Sep. 1995.

[11] F. C. Chen and H. K. Khalil, "Adaptive control of a class of nonlinear discrete-time systems using neural networks," *IEEE Trans. Autom. Control*, vol. 40, no. 5, pp. 791–801, May 1995.

[12] S. Jagannathan, "Control of a class of nonlinear systems using multilayered neural networks," *IEEE Trans. Neural Netw.*, vol. 12, no. 5, pp. 1113–1120, Sep. 2001.

[13] B. Igelnik and Y. H. Pao, "Stochastic choice of basis functions in adaptive function approximation and the functional-link net," *IEEE Trans. Neural Netw.*, vol. 6, no. 6, pp. 1320–1329, Nov. 1995.

[14] S. Jagannathan, "Robust backstepping control of robotic systems using neural networks," in *Proc. 37th IEEE Conf. Decision Control*, 1998, pp. 943–948.

[15] H. K. Khalil, *Nonlinear Systems*, 3rd ed. Englewood Cliffs, NJ: Prentice-Hall, 2002.

[16] P. He, Z. Chen, and S. Jagannathan, "Reinforcement learning based neural network control of nonstrict feedback nonlinear systems," in *Proc. IEEE Conf. Decision Control*, Dec. 2005, pp. 2580–2585.

[17] F. L. Lewis, S. Jagannathan, and A. Yesilderek, *Neural Network Control of Robot Manipulator and Nonlinear Systems*. London, U.K.: Taylor & Francis, 1999.

[18] F. L. Lewis, J. Campos, and R. Selmic, *Neuro-Fuzzy Control of Industrial Systems With Actuator Nonlinearities*. Philadelphia, PA: SIAM, 2002.

[19] S. Jagannathan, *Neural Network Control of Nonlinear Discrete-time Systems*. Boca Raton, FL: CRC Press, 2006.

Jonathan Blake Vance (S'04–M'05) was born on January 26, 1981, in Metairie, LA. He received the B.S. degree in computer engineering and the B.S. degree in electrical engineering, both in 2003, and the M.S. degree in computer engineering in 2005, all from the University of Missouri-Rolla, Rolla, where currently, he is working towards the Ph.D. degree in electrical engineering.

He is a member of the Eta Kappa Nu—Electrical and Computer Engineering Honor Society, and Tau Beta Pi—The Engineering Honor Society.

Atmika Singh received the M.S. degree in electrical engineering from the University of Missouri-Rolla (UMR), Rolla, in 2004, where currently, she is working towards the Ph.D. degree in systems engineering.

She is affiliated with the Laboratory for Investment and Financial Engineering at UMR. Her research interests include computational intelligence and risk modeling.

Brian C. Kaul was born on December 9, 1978, in St. Louis County, MO. He received the B.S. (*summa cum laude*) and M.S. degrees in mechanical engineering from the University of Missouri-Rolla, Rolla, in 2001 and 2003, respectively, where currently, he is working towards the Ph.D. degree in mechanical engineering.

Sarangapani Jagannathan (M'94–SM'99) received the B.S. degree from the College of Engineering, Guindy at Anna University, Madras, India, in 1987, the M.S. degree from the University of Saskatchewan, Saskatoon, Canada, in 1989, and the Ph.D. degree from the University of Texas, San Antonio, in 1994, all in electrical engineering.

From 1986 to 1987, he was a Junior Engineer at Engineers India Limited, New Delhi, India, a Research Associate and Instructor from 1990 to 1991 at the University of Manitoba, Winnipeg, Canada, and as a consultant from 1994 to 1998 at the Systems and Controls Research Division, Caterpillar Inc., Peoria. From 1998 to 2001, he was at the University

of Texas at San Antonio, and since September 2001, he has been at the University of Missouri-Rolla, Rolla, where currently, he is a Professor and Site Director for the National Science Foundation Industry/University Cooperative Research Center on Intelligent Maintenance Systems. He has coauthored more than 170 refereed conference and reviewed journal articles and several book chapters and three books: *Neural Network Control of Robot Manipulators and Nonlinear Systems*, (London, U.K.: Taylor & Francis, 1999), *Discrete-Time Neural Network Control of Nonlinear Discrete-Time Systems* (Boca Raton, FL: CRC Press, 2006), and *Wireless Ad Hoc and Sensor Networks: Performance, Protocols and Control* (Boca raton, FL: CRC Press, 2007, to be published). Currently, he holds 17 patents and several are in process. His research interests include adaptive and neural network control, computer/communication/sensor networks, prognostics, and autonomous systems/robotics.

Dr. Jagannathan received several gold medals. Additionally, he was the recipient of Region 5 IEEE Outstanding Branch Counselor Award in 2006, Faculty Excellence Award in 2006, St. Louis Outstanding Branch Counselor Award in 2005, Teaching Excellence Award in 2005, Caterpillar Research Excellence Award in 2001, Presidential Award for Research Excellence at UTSA in 2001, NSF CAREER award in 2000, Faculty Research Award in 2000, Patent Award in 1996, and Sigma Xi "Doctoral Research Award" in 1994. He has served and currently serving on the program committees of several IEEE conferences. He is an Associate Editor for the IEEE TRANSACTIONS ON CONTROL SYSTEMS TECHNOLOGY and the IEEE TRANSACTIONS ON NEURAL NETWORKS, and on several program committees. He is a member of Tau Beta Pi, Eta Kappa Nu, and Sigma Xi and IEEE Committee on Intelligent Control. Currently, he is serving as the Program Chair for the 2007 IEEE International Symposium on Intelligent Control, and Publicity Chair for the 2007 International Symposium on Adaptive Dynamic Programming.

James A. (Jim) Drallmeier received the Ph.D. degree in mechanical engineering from the University of Illinois at Urbana-Champaign, Urbana, in 1989.

He joined the faculty of the University of Missouri-Rolla, Rolla, in 1989, where currently, he is the Professor of Mechanical Engineering. He operates the Spray Dynamics and Internal Combustion Engine Laboratories. His research interests are in the fields of combustion, laser-based measurement systems and internal combustion engines. Current research includes studying two-phase flows, particularly sprays and thin shear-driven films and the dynamics of highly strained, dilute, intermittent combustion. He has been involved in developing and using laser-based diagnostic techniques for measuring spray and thin film dynamics over the past two decades. Additionally, he has been active in studying fuel systems and mixture preparation for advanced engine designs.